Online supplemental data

Crucial role for Nox2 and sleep deprivation in aircraft noise-induced vascular and cerebral oxidative stress, inflammation and gene regulation

Swenja Kröller-Schön[1], Andreas Daiber[1,2], Sebastian Steven[1], Matthias Oelze[1], Katie Frenis[1], Sanela Kalinovic[1], Axel Heimann[3], Frank P. Schmidt[1], Antonio Pinto[4], Miroslava Kvandova[5], Ksenija Vujacic-Mirski[1], Konstantina Filippou[1], Markus Dudek[6], Markus Bosmann[6], Matthias Klein[7], Tobias Bopp[7], Omar Hahad[1], Philipp Wild[4], Katrin Frauenknecht[8], Axel Methner[9], Erwin R. Schmidt[10], Steffen Rapp[4,10], Hanke Mollnau[11]*, Thomas Münzel[1,2]*¶

From the [1] Center for Cardiology, Cardiology I – Laboratory of Molecular Cardiology, University Medical Center of the Johannes Gutenberg-University Mainz, Mainz, Germany; [2] German Center for Cardiovascular Research (DZHK), Partner Site Rhine-Main; [3] Institute of Neurosurgical Pathophysiology, University Medical Center of the Johannes Gutenberg-University Mainz, Mainz, Germany; [4] Preventive Cardiology and Preventive Medicine, Center for Cardiology, University Medical Center of the Johannes Gutenberg-University Mainz, Mainz, Germany; [5] Institute of Normal and Pathological Physiology, Slovak Academy of Sciences, Bratislava, Slovakia; [6] Center for Thrombosis and Hemostasis, University Medical Center of the Johannes Gutenberg-University Mainz, Mainz, Germany; [7] Institute for Immunology, University Medical Center of the Johannes Gutenberg-University Mainz, Mainz, Germany; [8] Institute of Neuropathology, University Hospital, Zurich, Switzerland; [9] Department of Neurology, University Medical Center of the Johannes Gutenberg-University Mainz, Mainz, Germany; [10] Institute for Molecular Genetics, Johannes Gutenberg University, Mainz, Germany; [11] Center for Cardiology, Cardiology II – Rhythmology, University Medical Center of the Johannes Gutenberg-University Mainz, Mainz, Germany.

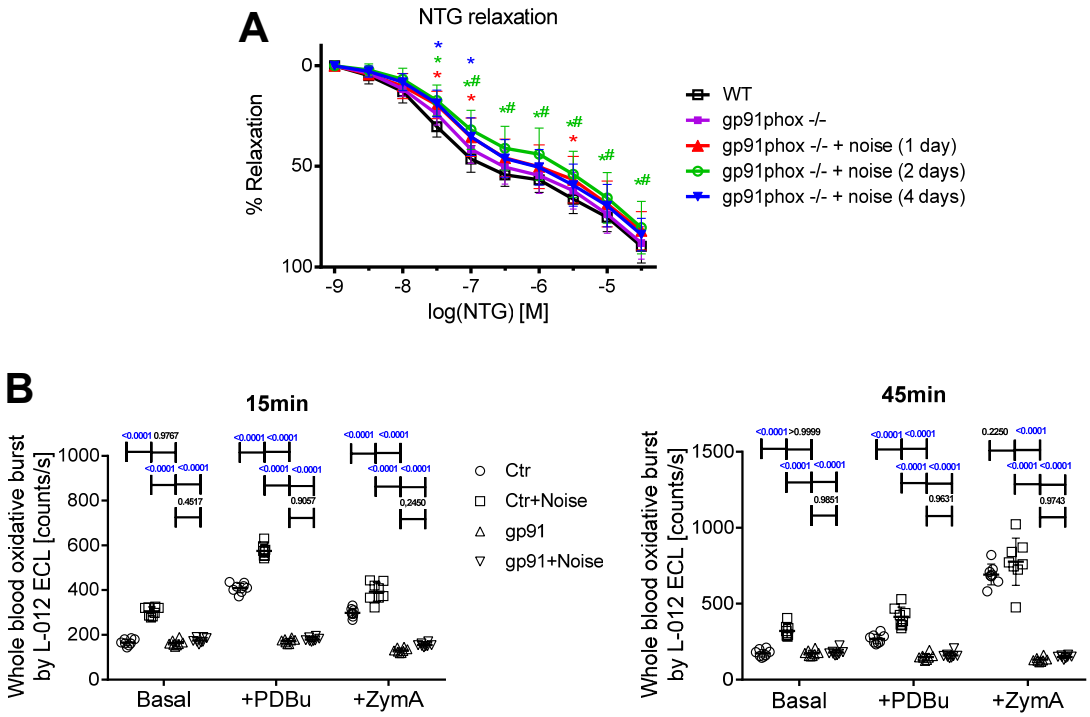

Suppl. Figure S1. Effects of *Nox2* (*gp91phox*) deficiency on around the clock noise exposure (24 h/d) induced alterations of endothelium-independent relaxation and whole blood oxidative burst. Endothelium-independent relaxation was tested by nitroglycerin (NTG) addition to isolated aortic rings of noise-exposed *Nox2*$^{-/-}$ mice by isometric tension measurement (**A**). Oxidative burst as a read-out for leukocyte activity was determined upon stimulation of whole blood (1:50 in PBS with 1 mM calcium/magnesium) with phorbol ester dibutyrate (PDBu, 10 µM) or zymosan A (ZymA, 50 µg/ml) by L-012 (100 µM) enhanced chemiluminescence. Oxidative burst was measured in samples from mice exposed to around the clock noise for 4 d. Data are mean ± SD from n = 9-16 mice/group (**A**) and 8 measurements with pooled samples from at least 3 mice/group (**B**). (**A**) Two-way ANOVA with Bonferroni's multiple comparisons test: *, $p<0.05$ versus WT without noise; $^{\#}$, $p<0.05$ versus gp91phox$^{-/-}$ without noise. (**B**) All data passed the normality test and One-way ANOVA with Tukey's correction was used.

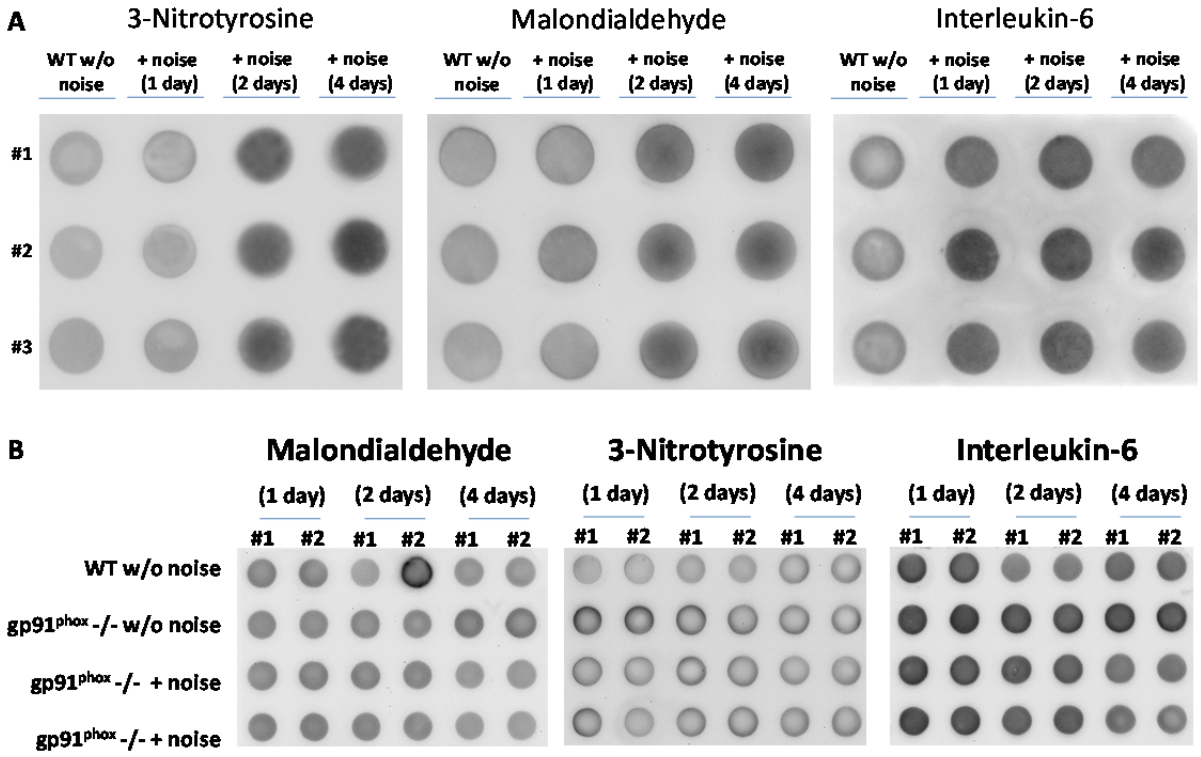

Suppl. Figure S2. Effects of continuous noise exposure (24 h/d) on systemic oxidative stress. Representative dot blots for data of **Figure 1D-F** in the main manuscript are shown for wild type and Nox2-/- (gp91phox-/-) mice exposed to around the clock aircraft noise.

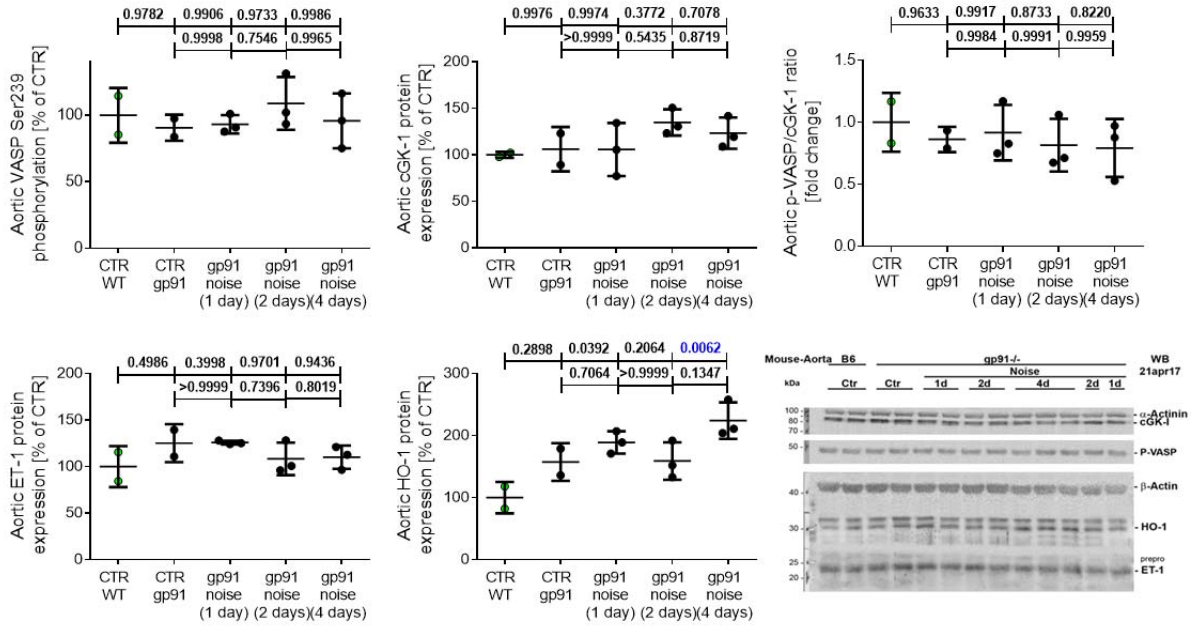

Suppl. Figure S3. Effects of *Nox2* (*gp91phox*) deficiency on around the clock noise exposure (24 h/d) induced alterations of aortic protein expression. Phosphorylation of VASP at serine 239 was not changed by around the clock noise exposure in *Nox2* (*gp91phox*) knockout mice (**A**). Expression levels of cGK-I were not changed by around the clock noise exposure in *Nox2* (*gp91phox*) knockout mice (**B**). The ratio of P-VASP to cGK-I, as a read-out for functional NO/cGMP signaling pathway, was not changed by around the clock noise exposure in *Nox2* (*gp91phox*) knockout mice (**C**). Expression levels of ET-1 were not changed by around the clock noise exposure in *Nox2* (*gp91phox*) knockout mice (**D**). Expression levels of HO-1 were not changed by around the clock noise exposure in *Nox2* (*gp91phox*) knockout mice (**E**). Representative Western blots are also shown (**F**). Data are mean ± SD from n = 2-3 samples/group (pooled from at least 3 mice per sample). All data passed the normality test and One-way ANOVA with Tukey's correction was used.

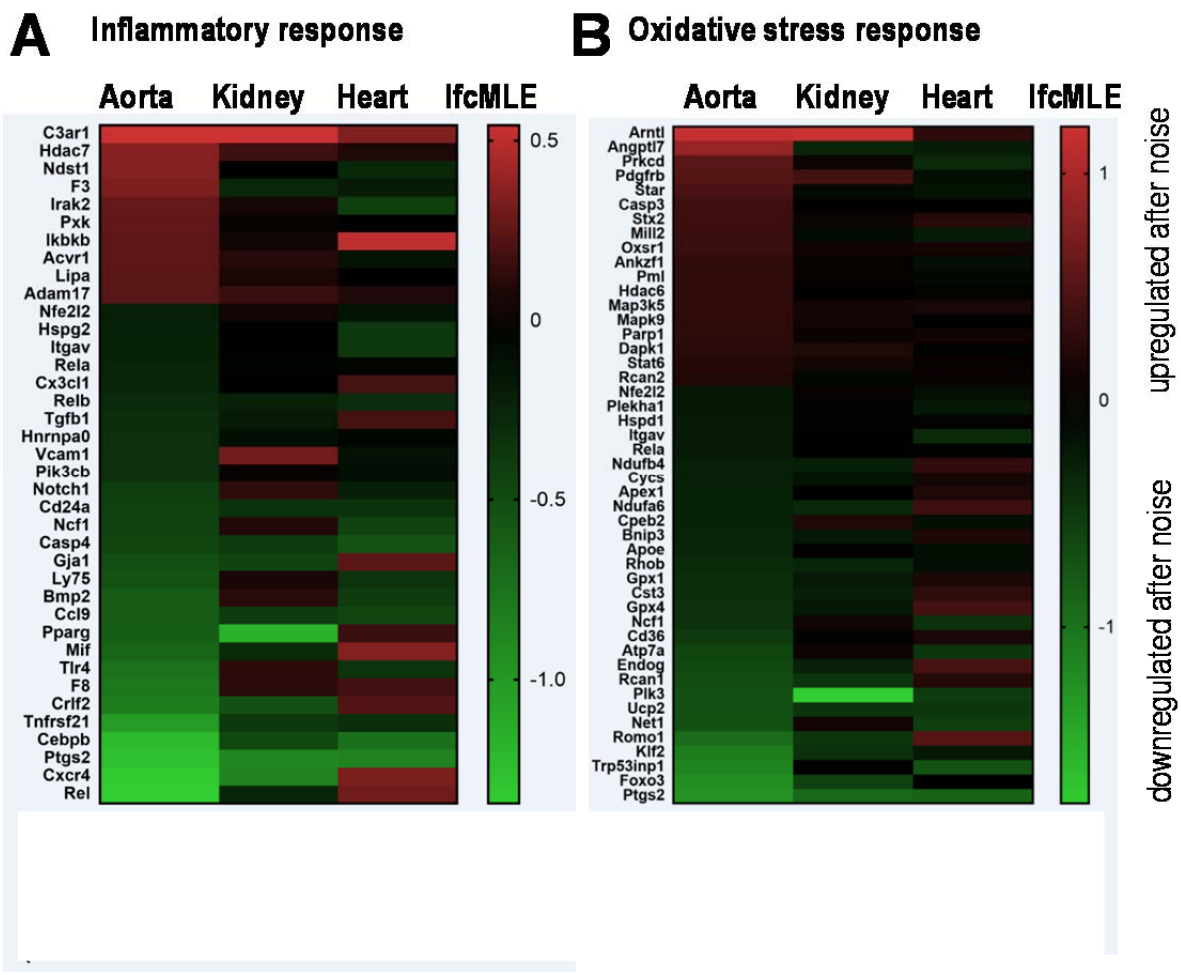

Suppl. Figure S4. Effects of around the clock noise exposure (24 h/d for 4 d) on gene expression profiles in different tissues. Changes of transcriptional profiles were determined by next generation sequencing in aorta, heart and kidney of mice exposed to aircraft noise. For better overview the genes were clustered into two heat maps highlighting transcriptional changes in inflammation and oxidative stress response. Next generation sequencing was performed with n=4 samples/group and each sample was pooled from 4 animals.

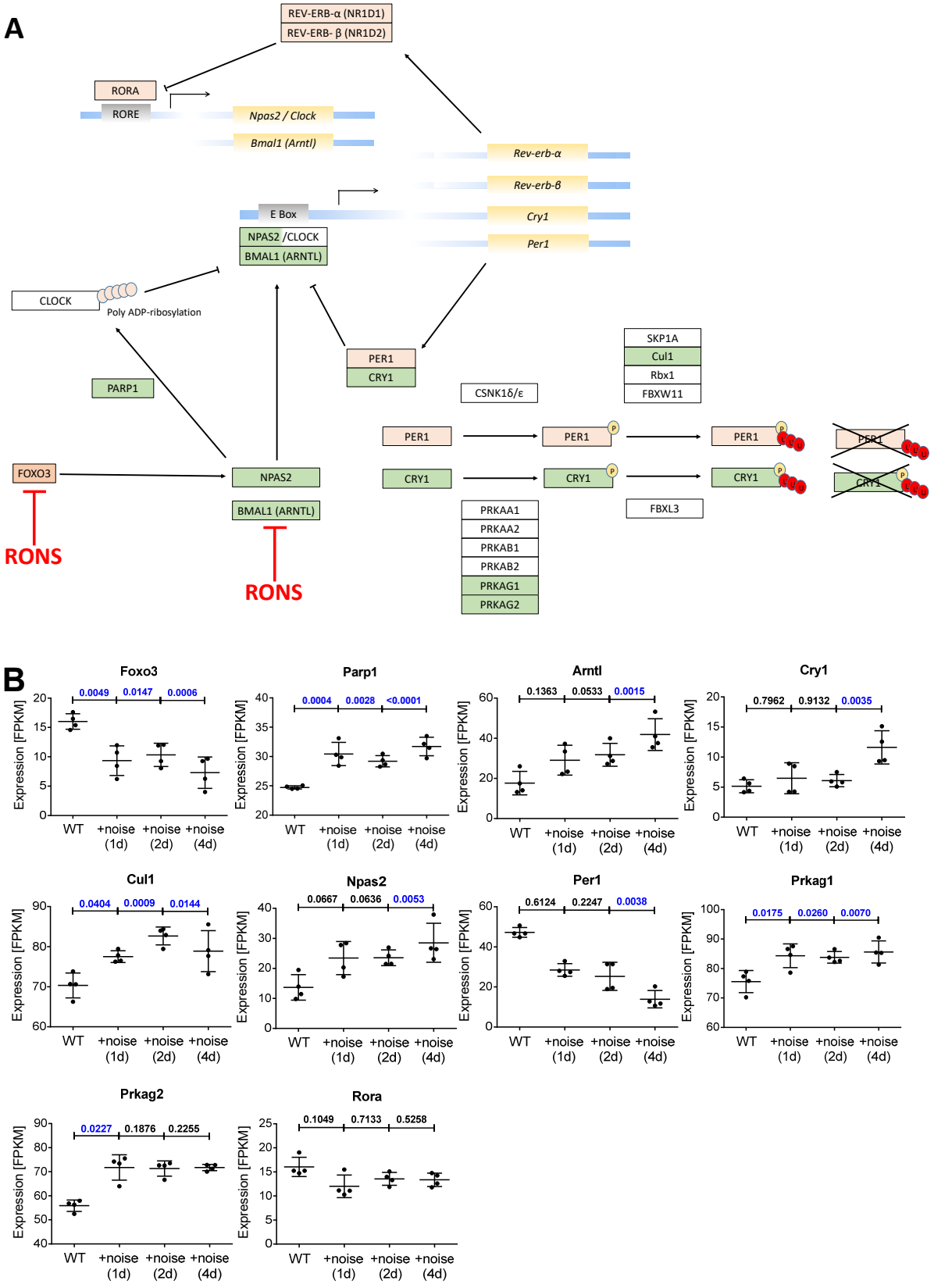

Suppl. Figure S5. Next generation sequencing reveals alterations in circadian clock genes by around-the-clock (24 h/d) noise exposure. (**A**) Aortic tissue was subjected to NGS. Genes with significantly changed expression after 1, 2 or 4 days of noise exposure are

marked with green (upregulation) or red (downregulation) color. A pathway map was generated by the NGS data by bioinformatic procedures. The circadian clock is a complex system based on a group of transcription factors regulated by posttranslational modifications and regulatory feedback loops. Key genes like *Foxo3, Per1, Bmal1* (*Arntl*), *Cry1, Npas2* (paralog of *Clock*) and *Rora* showed significant changes in gene expression after noise exposure. This also applies to other regulatory factors like *Parp1, Cul1, Prkag1/2*, which are involved in posttranslational modifications of the transcription factor. Phosphorylation and ubiquitinylation, which lead to increased proteasomal degradation are important regulatory processes for their stability and activity. (**B**) Detailed information on time courses of gene expression. Data are mean ± SD of n=4 for each group; *Per1, Prkag2, Rora*: Normality test failed and non-parametric Kruskal-Wallis test with Dunn's correction was used. For all other data: Normality test passed and One-way ANOVA with Tukey's correction was used. Abbreviations: NPAS2, neuronal PAS domain protein 2; ARNTL/BMAL1, brain and muscle aryl hydrocarbon receptor nuclear translocator (ARNT)-like (BMAL) 1; PARP1, poly(ADP-ribose) polymerase 1; CRY-1, cryptochrome circadian clock 1; PER1, period circadian clock 1; PRKAG1/2, protein kinase AMP-activated non-catalytic subunit gamma 1/2; Cul1, cullin 1; REV-ERB-α (NR1D1), nuclear receptor subfamily 1 group D member 1; REV-ERB-β (NR1D2), nuclear receptor subfamily 1 group D member.

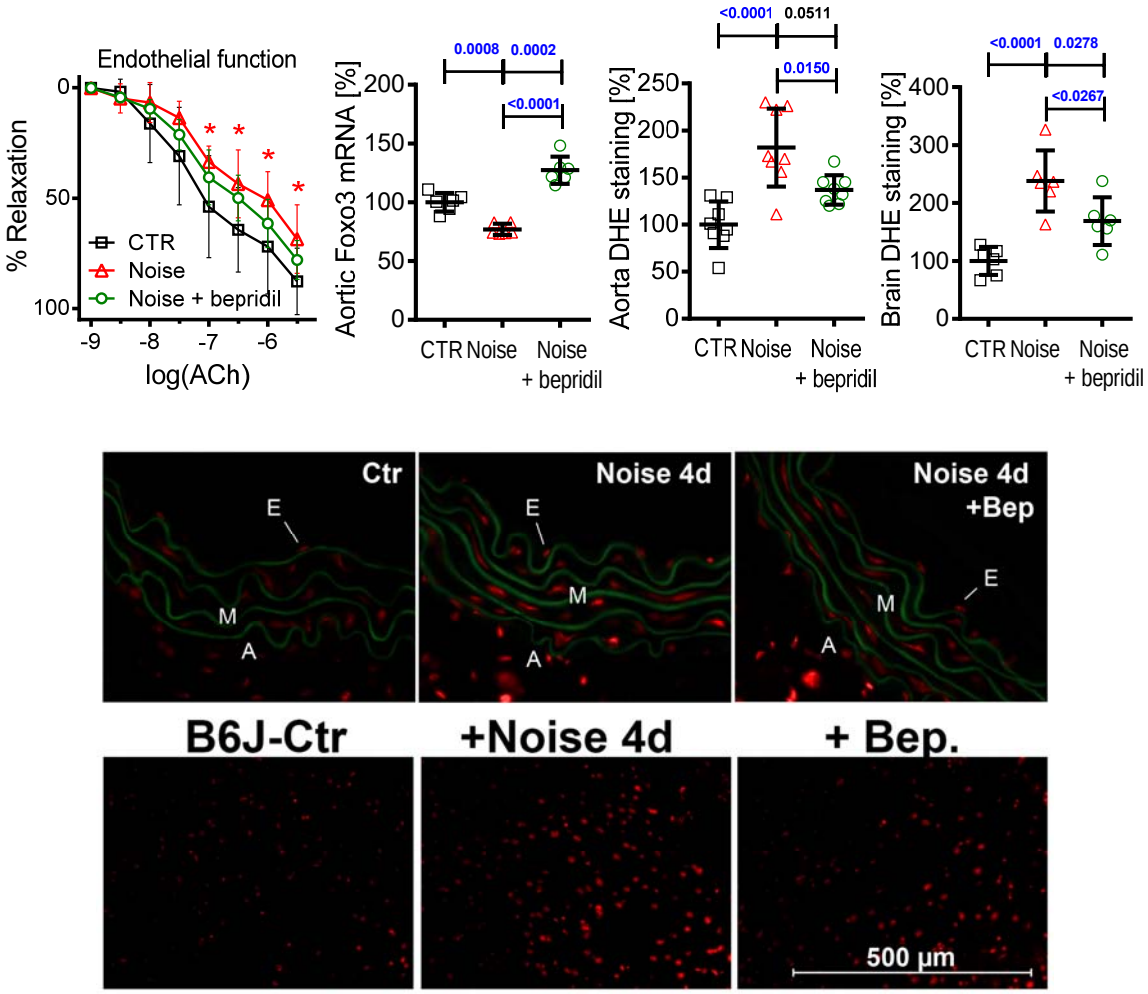

Suppl. Figure S6. Effects of around the clock noise exposure (24 h/d for 4 d) and bepridil co-treatment (20 mg/kg/d for 5 d, once daily by i.p. injection) on endothelial function, *Foxo3* mRNA expression and vascular/cerebral ROS formation. Activation of *Foxo3*, a key regulator of antioxidant defense and circadian rhythm, by the calcium antagonist and anti-anginal drug bepridil improved endothelial function (ACh-dependent relaxation measured by ismetric tension methodology), *Foxo3* mRNA expression and vascular as well as cerebral oxidative stress in noise-exposed mice. Cryo-sections of the aorta and the frontal cortex were stained with dihydroethidium (1 µM) for detection of cytosolic/cellular ROS formation. Representative pictures are shown for all groups. Data are mean ± SD from 6-9 mice/group. . Vascular function: Two-way ANOVA with Bonferroni's multiple comparisons test: *, $p<0.05$ versus WT without noise. Expression and ROS formation: All data passed the normality test and One-way ANOVA with Tukey's correction was used.

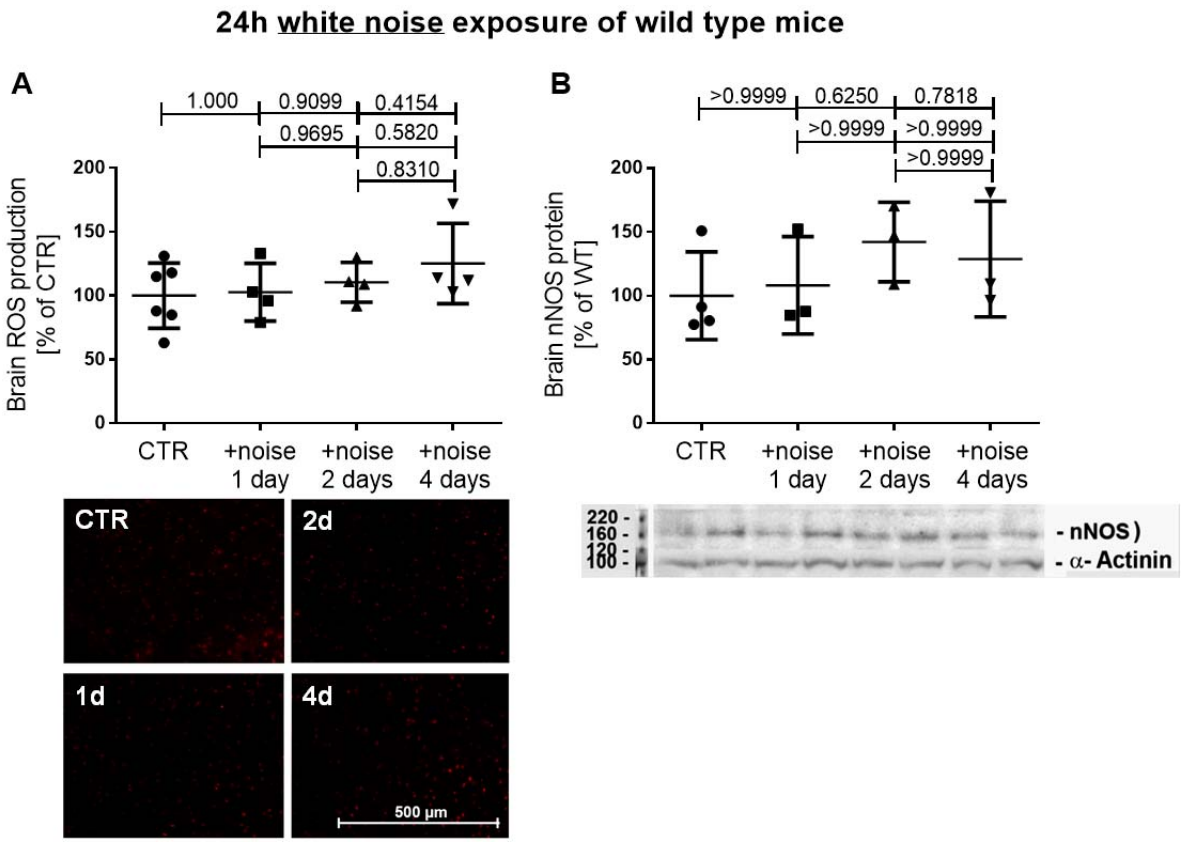

Suppl. Figure S7. Effects of around the clock white noise exposure (24 h/d) on cerebral ROS formation and nNOS expression. (**A**) Cryo sections of the frontal cortex were stained with dihydroethidium. Exposure of wild type mice to around-the-clock white noise induced no cerebral ROS formation. (**B**) Protein expression of nNOS was assessed by Western blotting using specific antibody against nNOS and was not altered by around-the-clock exposure to white noise. Representative pictures and blots are shown for all groups. Data are mean ± SD from at least 4 mice/group. (**A**) Normality test passed and One-way ANOVA with Tukey's correction was used. (**B**) Normality test failed and non-parametric Kruskal-Wallis test with Dunn's correction was used.

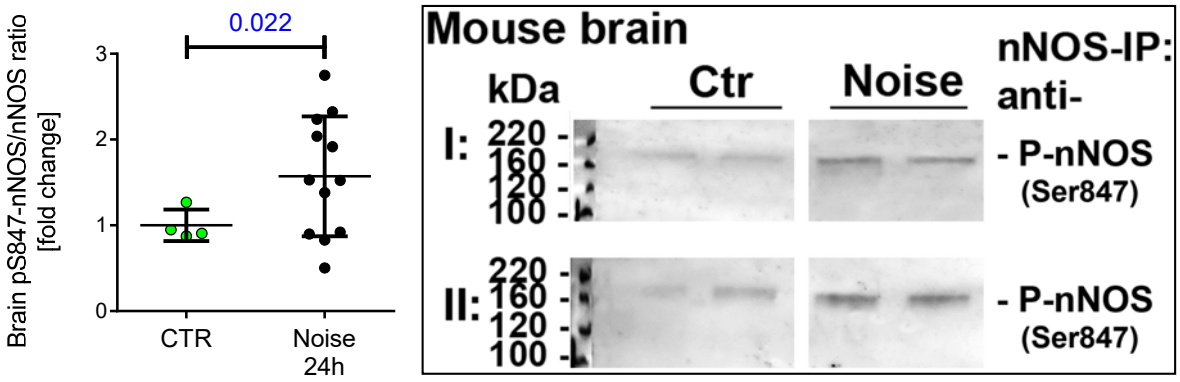

Suppl. Figure S8. Effects of around the clock noise exposure (24 h/d) on cerebral nNOS phosphorylation at Ser847. Phosphorylation was assessed in brain homogenates by immunoprecipitation of nNOS followed by Western blotting for pS847-nNOS. After striping the blot it was stained for nNOS. Representative blots are shown beside the densitometric quantification. Data are mean ± SD from 4 samples per group (each pooled from 2-3 mice). Unpaired t-test with Welch's was used for statistical analysis since equal variance test failed.

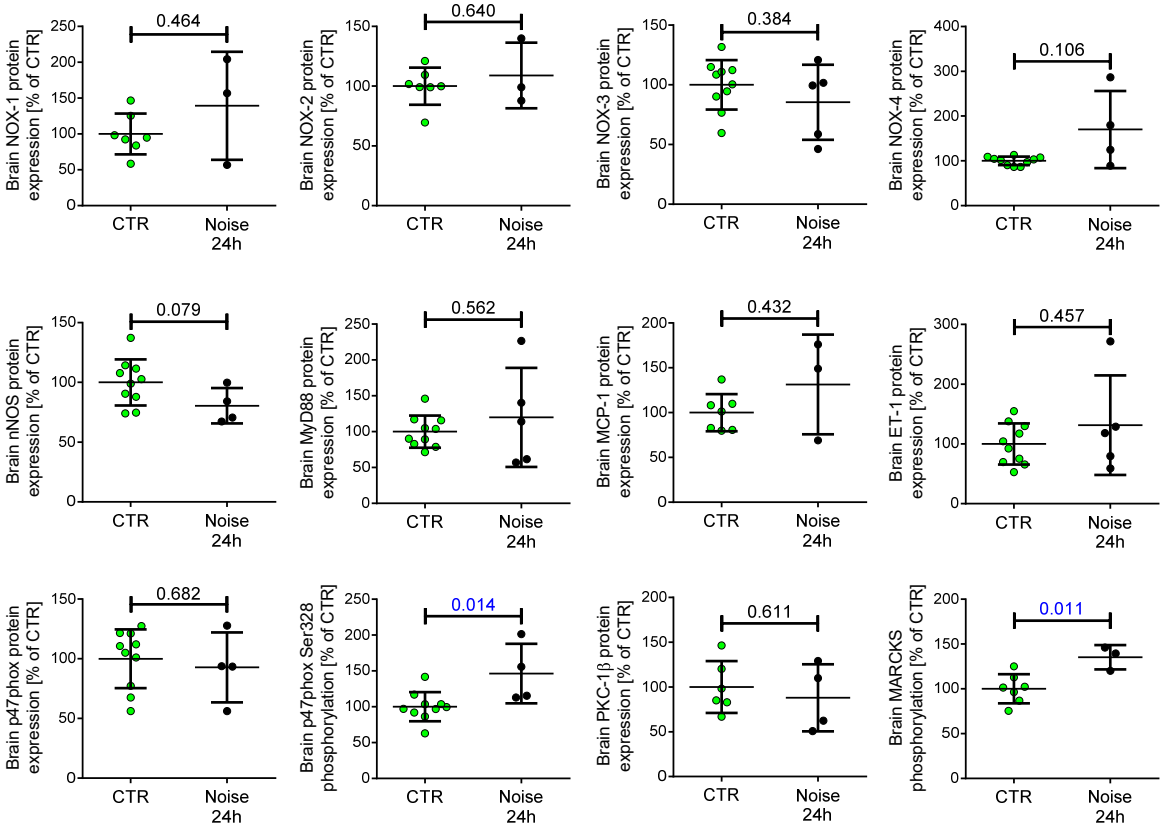

Suppl. Figure S9. Effects of around the clock noise exposure (24 h/d for 4 d) on protein expression in the frontal cortex. Expression levels of the ROS sources Nox1, Nox2, Nox3 and Nox4, nNOS, the mediators of inflammation MyD88, MCP-1, the vasoconstrictor endothelin-1, protein kinase C (PKC) and its activity marker phospho-MARCKS, as well as p47phox and its PKC-specific phosphorylation at serine 328 were assessed by Western blot analysis. Data are mean ± SD from n = 3 samples/group (pooled from at least 2 mice per sample). Unpaired t-test (with Welch's correction when equal variance test failed) and Mann Whitney test on ranks (when normality test failed) was used for statistical analysis.

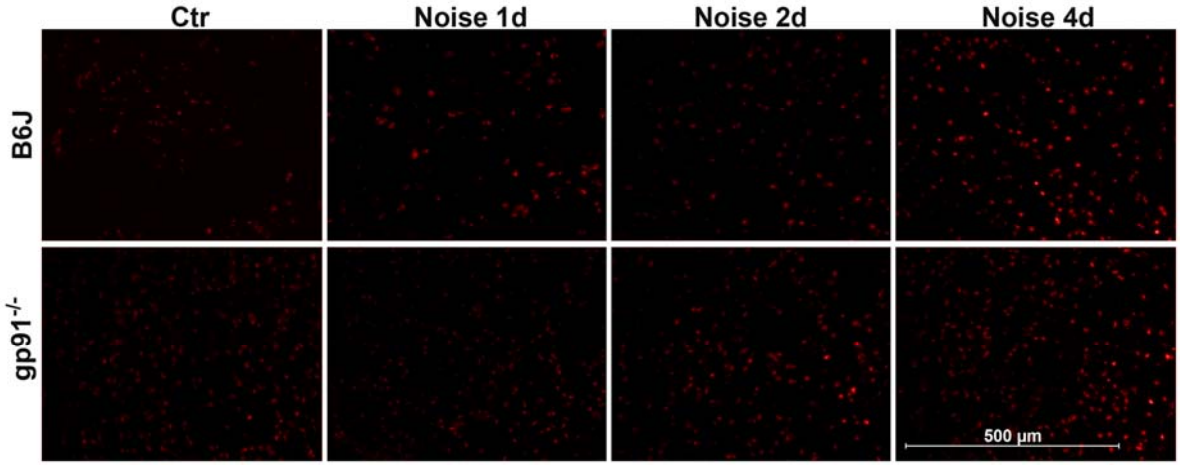

Suppl. Figure S10. Effects of around the clock noise exposure (24 h/d for 1, 2 and 4 d) on cerebral mitochondrial ROS formation. Representative pictures are shown for the data presented in **Figure 2I**.

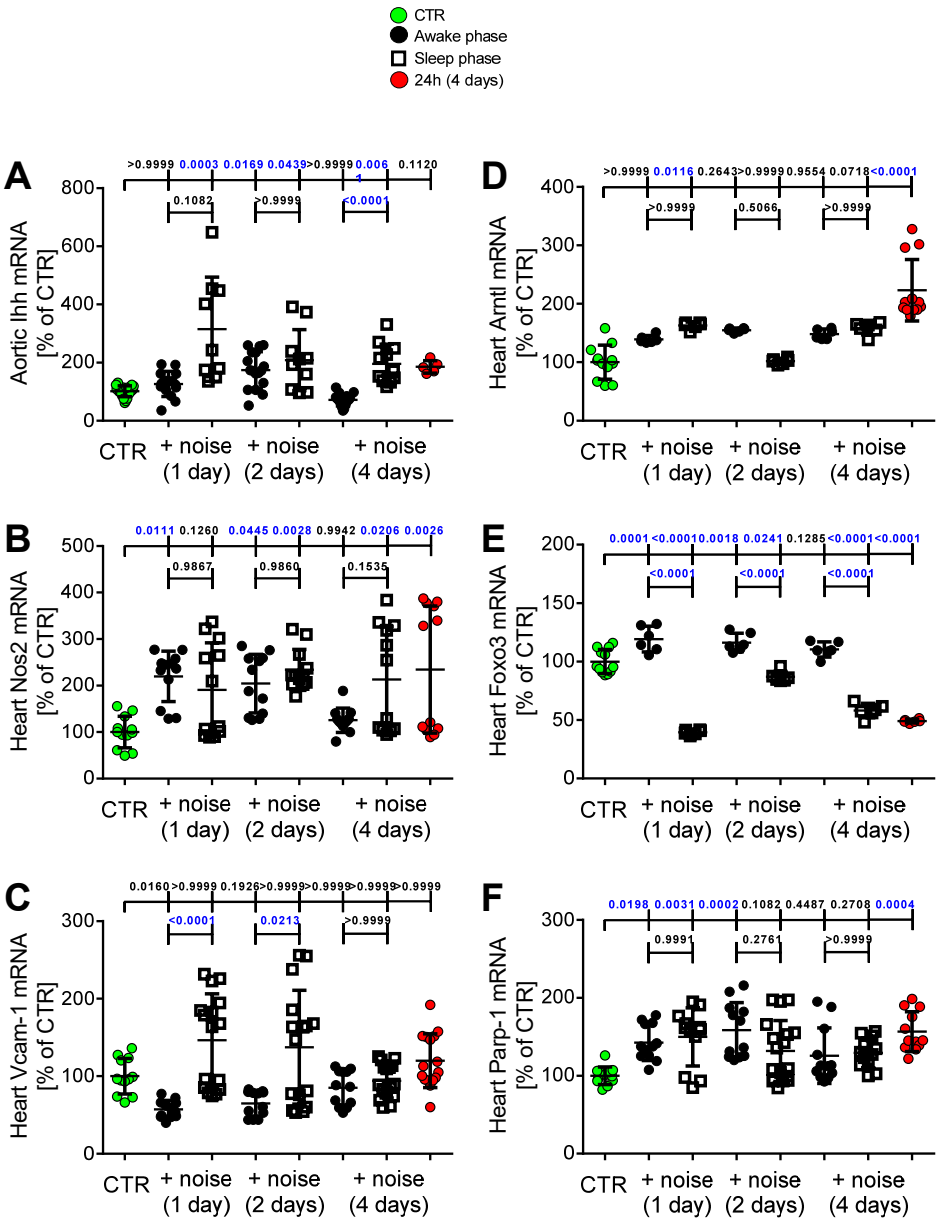

Suppl. Figure S11. Effects of noise exposure during the sleep or awake phase (12 h/d) on gene expression (RT-PCR data). Expression of *indian hedgehog* (*Ihh*) mRNA (**A**), the inflammatory genes *iNOS* (*Nos2*) and *Vcam1* (**B-C**), the circadian clock gene *Arntl* (**D**), the transcription factor *Foxo3* (**E**) and *poly(ADP-ribose) polymerase 1* (*Parp-1*) (**F**) was assessed by RT-PCR to compare the gene modulatory effects of awake and sleep phase versus around-the-clock noise exposure. The last bar in each graph (marked with red color) is the reference value of mice exposed to around-the-clock aircraft noise for 4 days. Data are mean±SD from n=6 (**A-F**) mice/group. (**A,C,D**) Normality test failed and non-parametric Kruskal-Wallis test with Dunn's correction was used. (**B,E,F**) Normality test passed and One-way ANOVA with Tukey's correction was used.

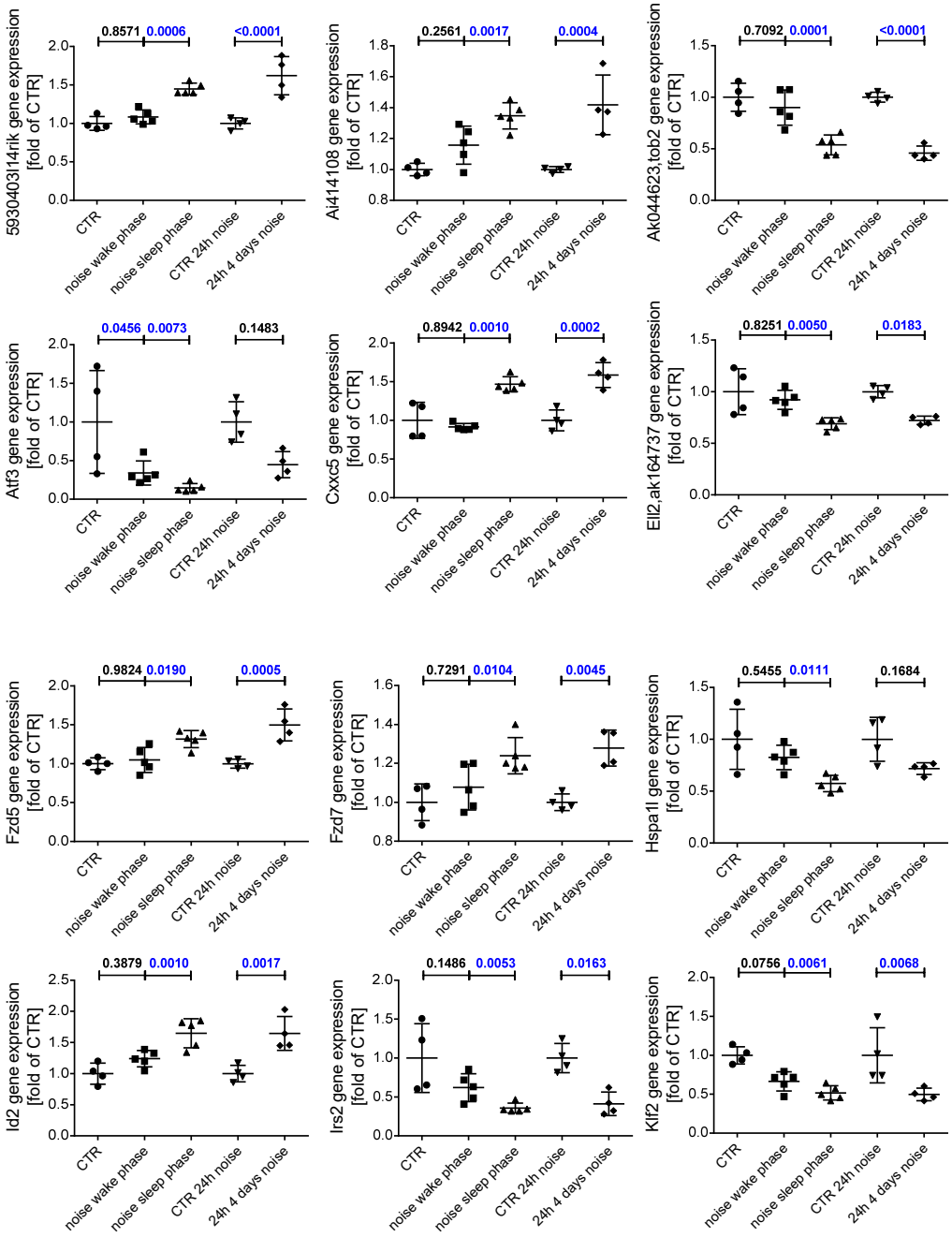

Suppl. Figure S12. Next generation sequencing reveals similarities in gene regulation by around-the-clock (24 h/d) and sleep phase noise exposure. Aortic tissue was subjected to NGS. Gene expression was assessed after 4 days of noise exposure (sleep / awake phase or 24h). NGS analysis in sleep/awake phase and 24h exposures represented two independent datasets. For comparison of these different datasets noise exposure data of sleep/awake phase and 24h groups were normalized to the respective unexposed controls, expressed as % of control and subjected to One-way ANOVA analysis. Data are mean ± SD of n=4 for each group and each sample was pooled from 4 animals; All data passed the normality test and One-way ANOVA with Tukey's correction was used.

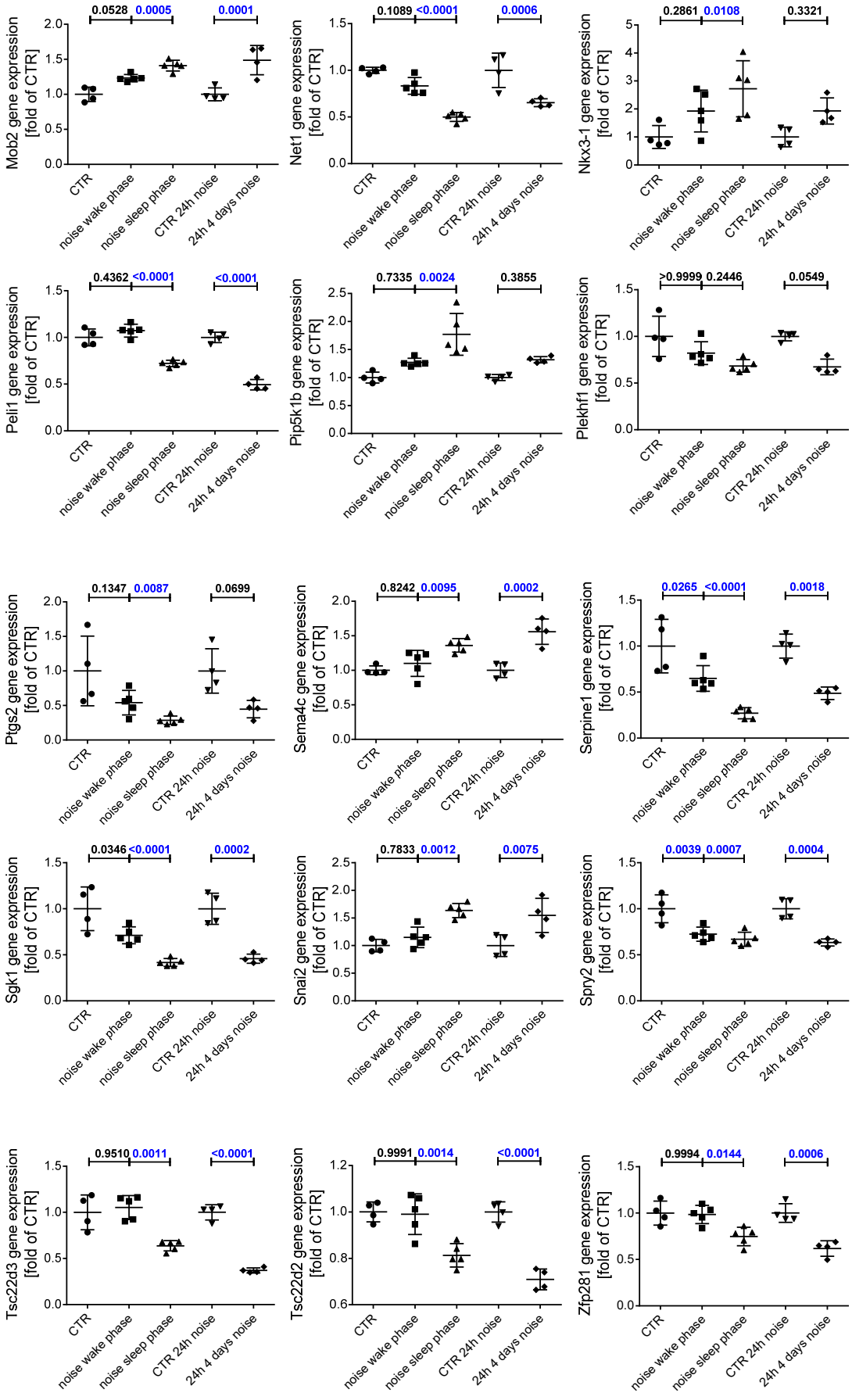
Mob2 gene expression [fold of CTR]
0.0528 0.0005 0.0001
Net1 gene expression [fold of CTR]
0.1089 <0.0001 0.0006
Nkx3-1 gene expression [fold of CTR]
0.2861 0.0108 0.3321
Peli1 gene expression [fold of CTR]
0.4362 <0.0001 <0.0001
Pip5k1b gene expression [fold of CTR]
0.7335 0.0024 0.3855
Plekhf1 gene expression [fold of CTR]
>0.9999 0.2446 0.0549
Ptgs2 gene expression [fold of CTR]
0.1347 0.0087 0.0699
Sema4c gene expression [fold of CTR]
0.8242 0.0095 0.0002
Serpine1 gene expression [fold of CTR]
0.0265 <0.0001 0.0018
Sgk1 gene expression [fold of CTR]
0.0346 <0.0001 0.0002
Snai2 gene expression [fold of CTR]
0.7833 0.0012 0.0075
Spry2 gene expression [fold of CTR]
0.0039 0.0007 0.0004
Tsc22d3 gene expression [fold of CTR]
0.9510 0.0011 <0.0001
Tsc22d2 gene expression [fold of CTR]
0.9991 0.0014 <0.0001
Zfp281 gene expression [fold of CTR]
0.9994 0.0144 0.0006
CTR
noise wake phase
noise sleep phase
CTR 24h noise
24h 4 days noise

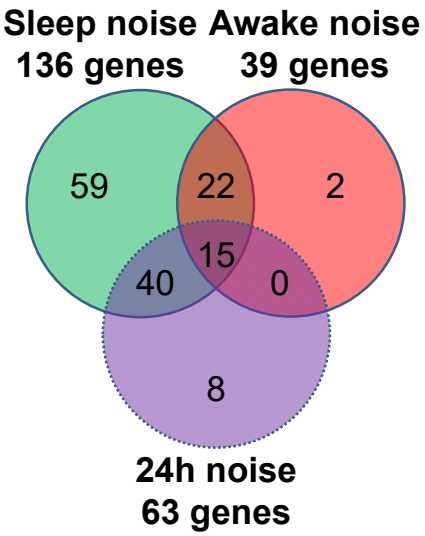

Suppl. Figure S13. Next generation sequencing reveals similarities in gene regulation by around-the-clock (24 h/d) and sleep phase noise exposure. Aortic tissue was subjected to NGS. Gene expression was assessed after 4 days of noise exposure (sleep / awake phase or 24h). NGS analysis in sleep/awake phase and 24h exposures represented two independent datasets. For comparison of these different datasets noise exposure data of sleep/awake phase and 24h groups were normalized to the respective unexposed controls, expressed as % of control and subjected to One-way ANOVA analysis. Data are mean ± SD of n=4 for each group and each sample was pooled from 4 animals; *Pip5k1b, Plekhf1*: Normality test failed and non-parametric Kruskal-Wallis test with Dunn's correction was used. For all other data: Normality test passed and One-way ANOVA with Tukey's correction was used.

The pie chart summarizes the results of comparisons of the 3 different noise exposure protocols. NGS analysis revealed 196 significantly regulated genes in the sleep phase noise group. 183 of these genes were also found by NGS analysis in response to the other noise exposure protocols. 20 of these genes were not significantly regulated in any of the three noise exposure protocol groups by One-way ANOVA analysis. 17 of these genes were regulated differentially in sleep phase versus 24h groups (one up- and one downregulated). The remaining 146 genes were assessed for significant synergistic regulation among the three noise exposure protocol groups by One-way ANOVA analysis and the results are displayed in the pie chart.

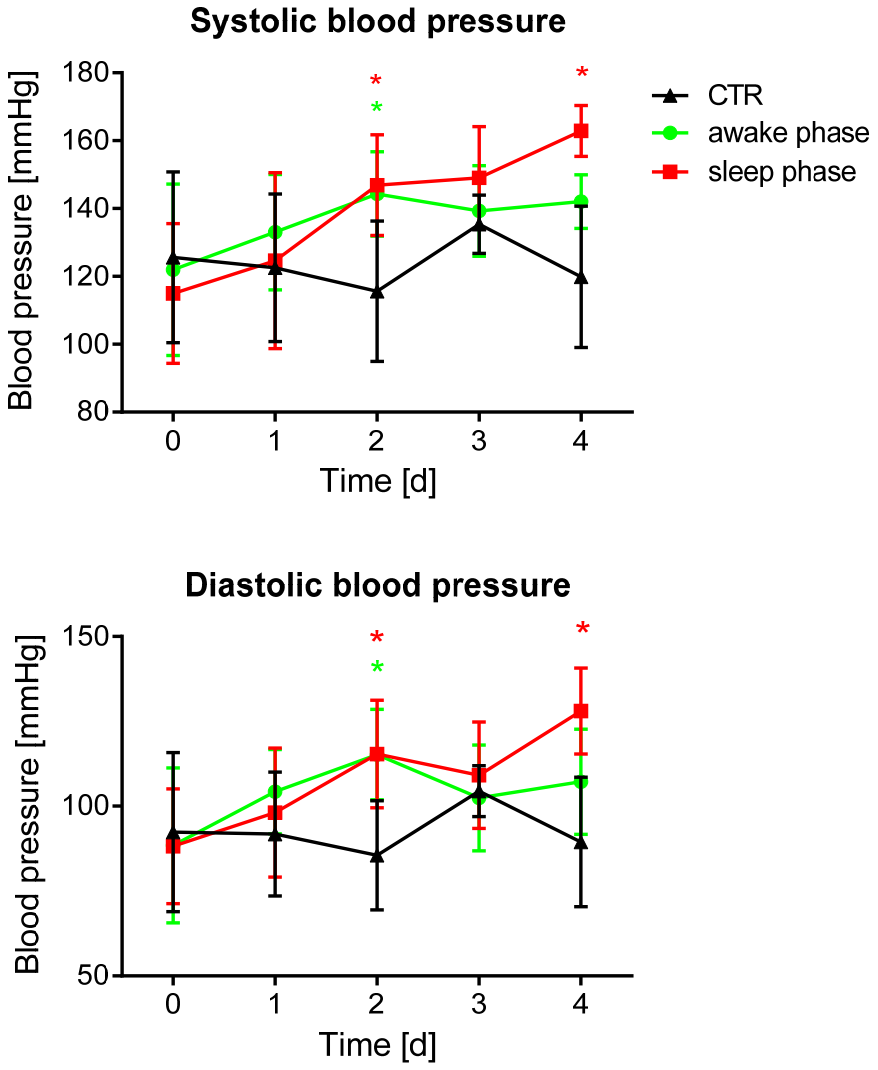

Suppl. Figure S14. Time-dependent changes of blood pressure in response to noise exposure during the sleep or awake phase (12 h/d). Blood pressure was measured by tail cuff measurements. Systolic and diastolic blood pressure was increased after sleep and awake phase noise exposure for 4 d. The increase of blood pressure was more pronounced after sleep phase noise exposure. Data are mean ± SD from n = 3-5 mice per group. *, $p<0.05$ versus control without noise or versus awake phase exposed group on same day (as indicated by color code). Two-way ANOVA with Bonferroni's multiple comparisons test.

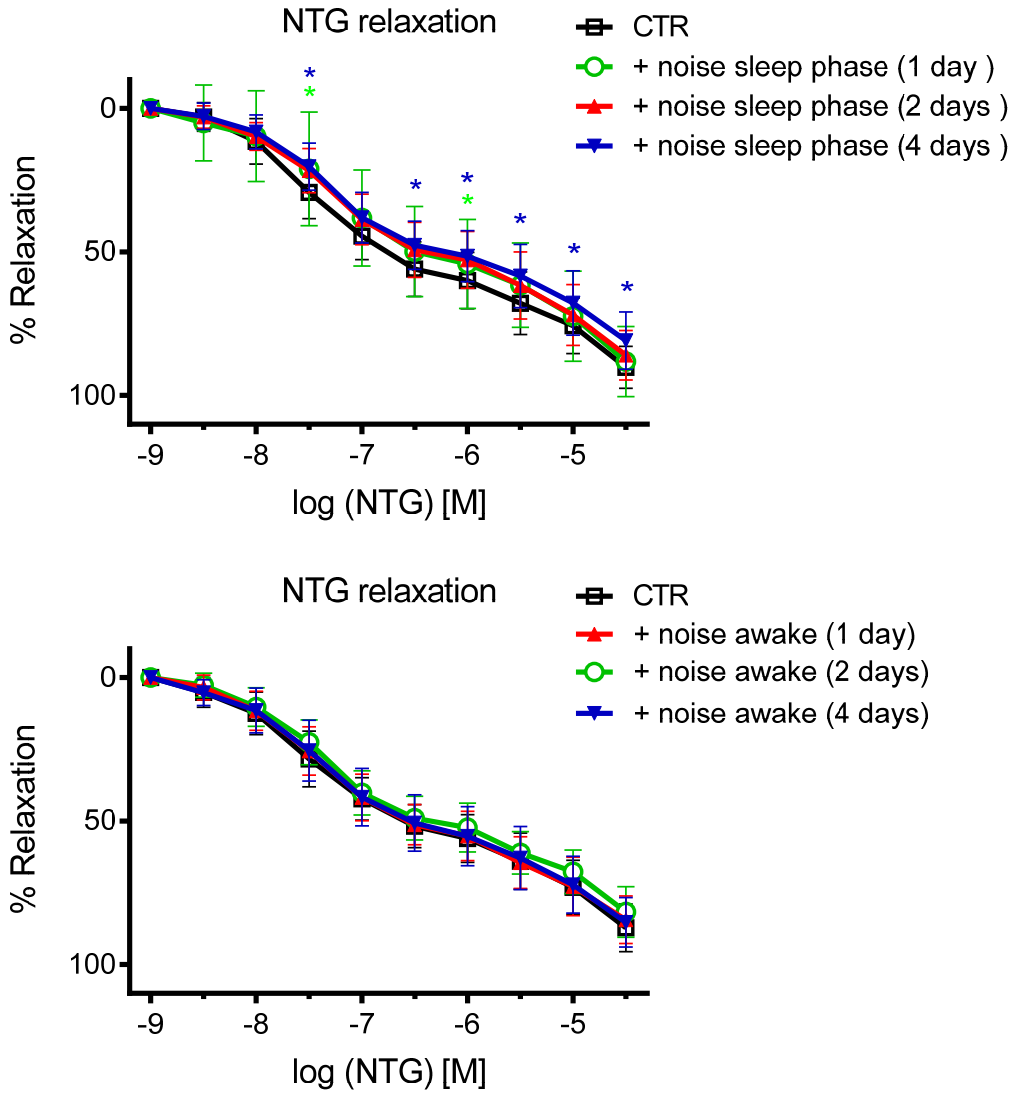

Suppl. Figure S15. Effects of noise exposure during the sleep or awake phase (12 h/d) on vascular function. Vascular function was determined by isometric tension measurements. Relaxation of isolated aortic ring segments by the endothelium-independent vasodilator nitroglycerin (NTG) was impaired by sleep phase but not awake phase noise exposure. Data are mean ± SD from n = 10-24 (sleep phase) and 18 (awake phase) mice per group. Two-way ANOVA with Bonferroni's multiple comparisons test: *, $p<0.05$ versus control without noise at the same NTG concentration (as indicated by color code).

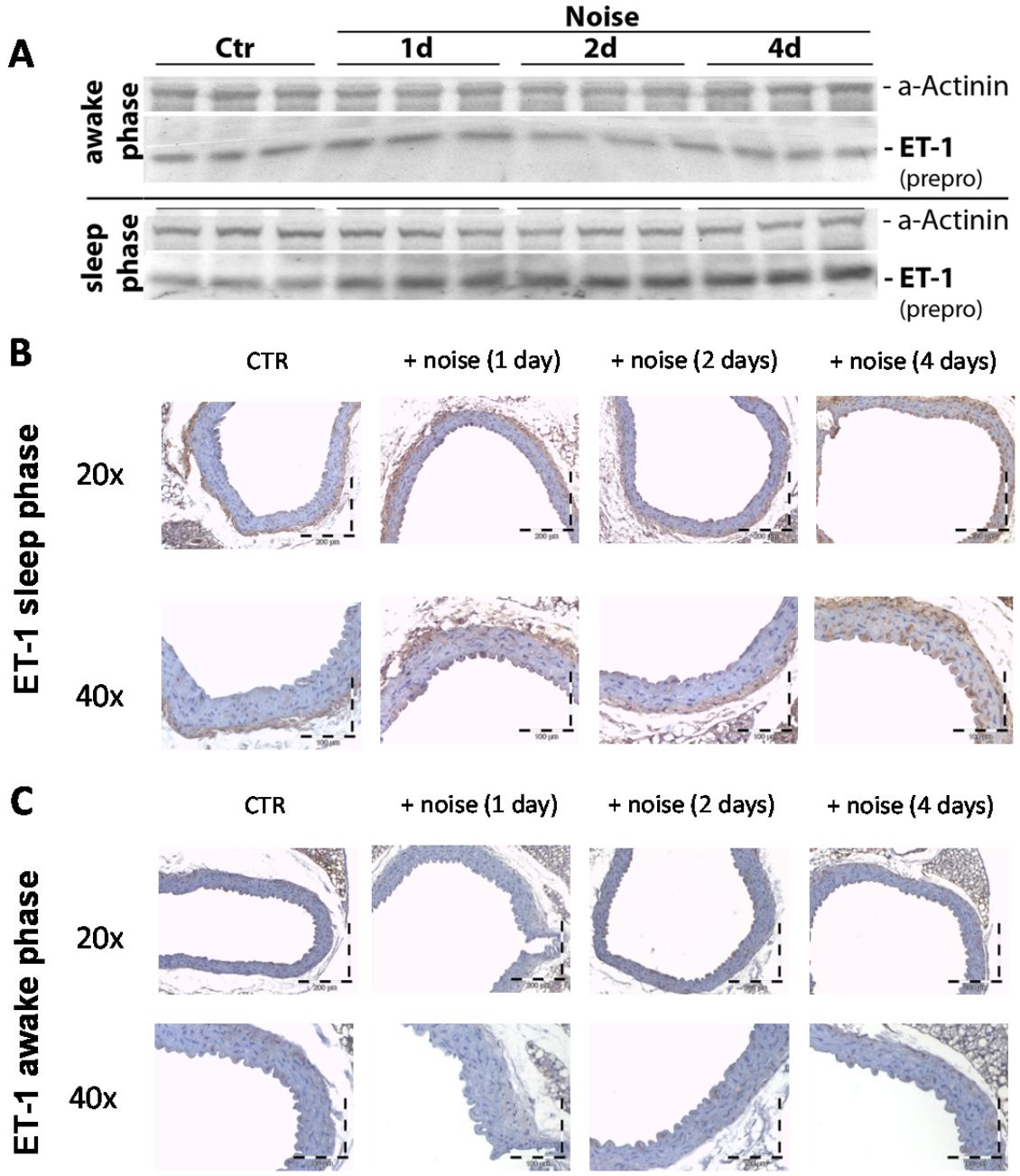

Suppl. Figure S16. Effects of sleep and awake phase noise exposure (12 h/d) on vascular endothelin-1 expression. Original Western blots of aortic ET-1 protein expression are shown for data of **Figure 4E** in the main manuscript (**A**). Immunohistochemical analysis revealed that noise exposure during the sleep phase (**B**) but not the awake phase (**C**) caused an increase in the expression of ET-1 in aortic tissue. Representative immunohistochemical images are shown for data of **Figure 4F** in the main manuscript.

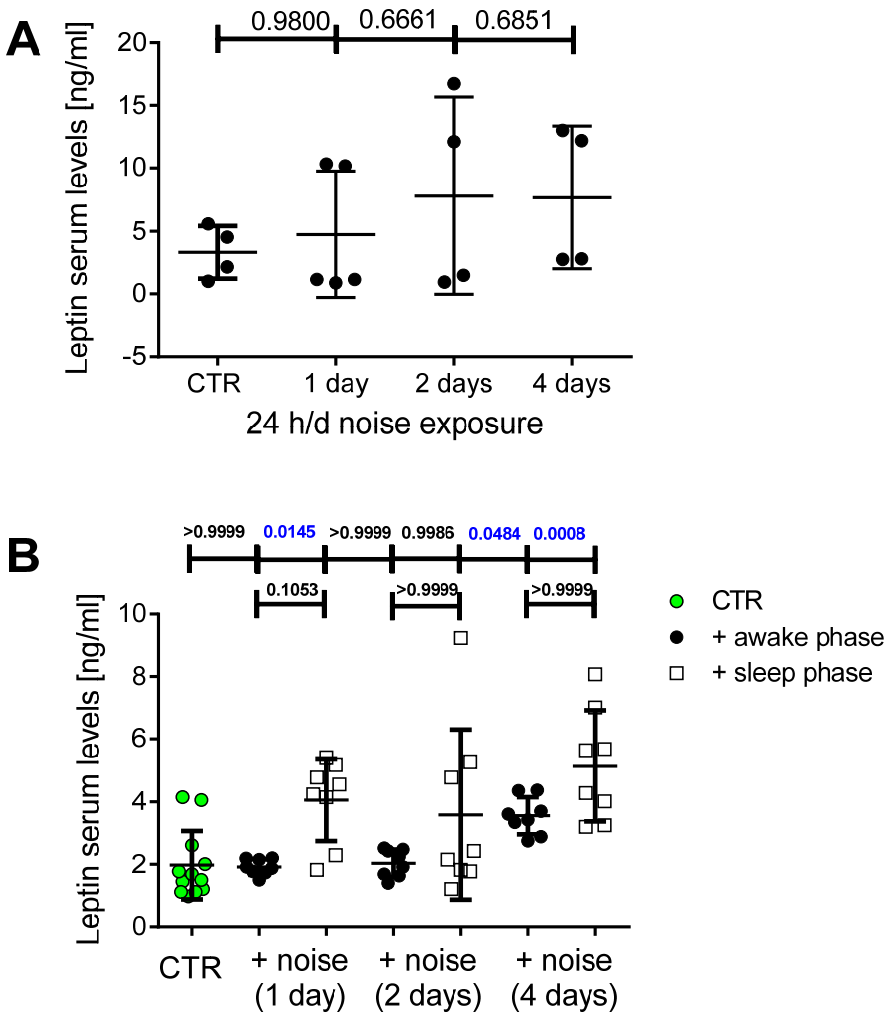

Suppl. Figure S17. Effects of noise exposure around the clock or during the sleep or awake phase (12 h/d) on expression of leptin levels. Serum leptin levels were increased by trend in response to around the clock noise exposure (**A**). Serum leptin levels were augmented after 1 and 4 days of sleep phase noise exposure (grey bars), whereas the awake phase exposure (black bars) had only an effect on day 4, which was also less pronounced as compared to sleep phase exposure (**B**). Data are mean ± SD from n = 4-5 (**A**) and 8-12 (**B**) mice/group. (**A**) Normality test passed and One-way ANOVA with Tukey's correction was used. (**B**) Normality test failed and non-parametric Kruskal-Wallis test with Dunn's correction was used.

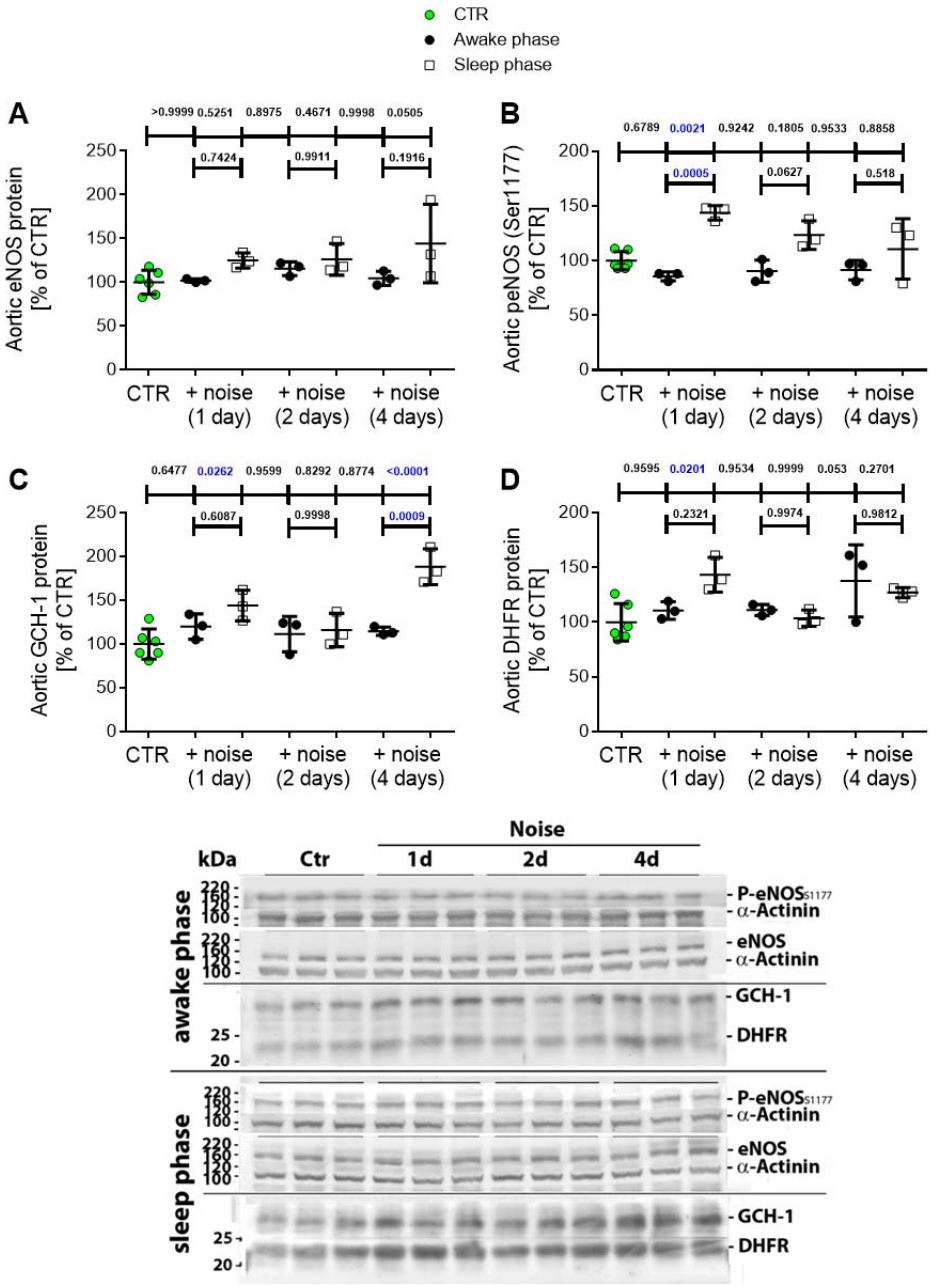

Suppl. Figure S18. Effects of sleep and awake phase noise exposure (12 h/d) on vascular $^{\bullet}$NO signaling pathway. Levels of aortic eNOS in response to sleep phase exposure shows a minor upregulation trend over all days, but not during awake phase noise exposure (**A**). Phosphorylation of eNOS at Ser1177 was significantly elevated on day 1 and 2 of sleep phase exposure (**B**). The expression of GCH-1 is significantly upregulated after 1 and 4 days of sleep phase noise exposure, but not after awake phase noise exposure (**C**). DHFR was upregulated significantly after 1 day sleep phase noise exposure (**D**). Representative Western blots are shown below the densitometric quantifications. Data are mean ± SD from n = 3-6 samples (pooled from 2-3 mice per sample). All data passed the normality test and One-way ANOVA with Tukey's correction was used.

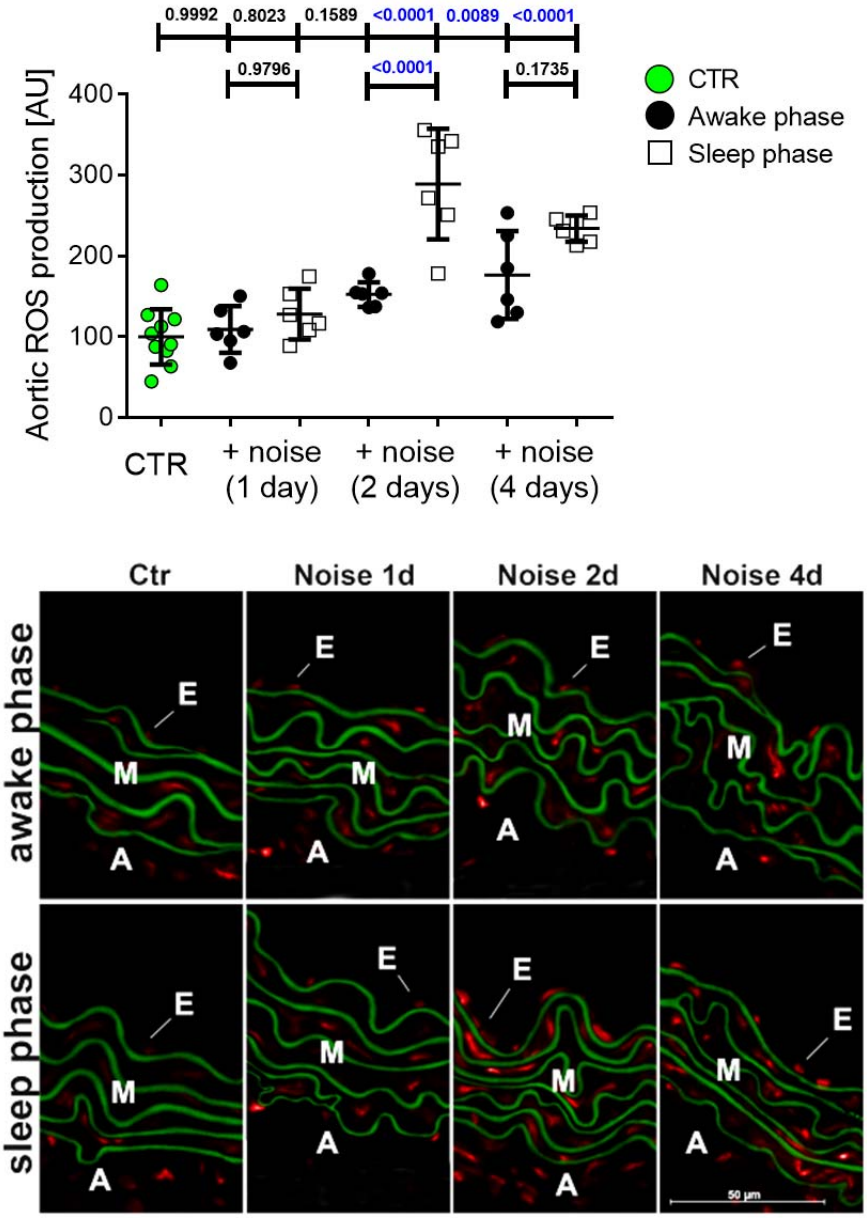

Suppl. Figure S19. Effects of sleep and awake phase noise exposure (12 h/d) on global vascular oxidative stress. In vascular tissue, sleep phase noise exposure increased ROS production on day 2 and 4 in a more pronounced way than awake phase noise exposure as revealed by DHE cryo staining. Representative stained images are shown together with the densitometric quantification. Data are mean ± SD from n = 6-10 mice/group. Normality test passed and One-way ANOVA with Tukey's correction was used.

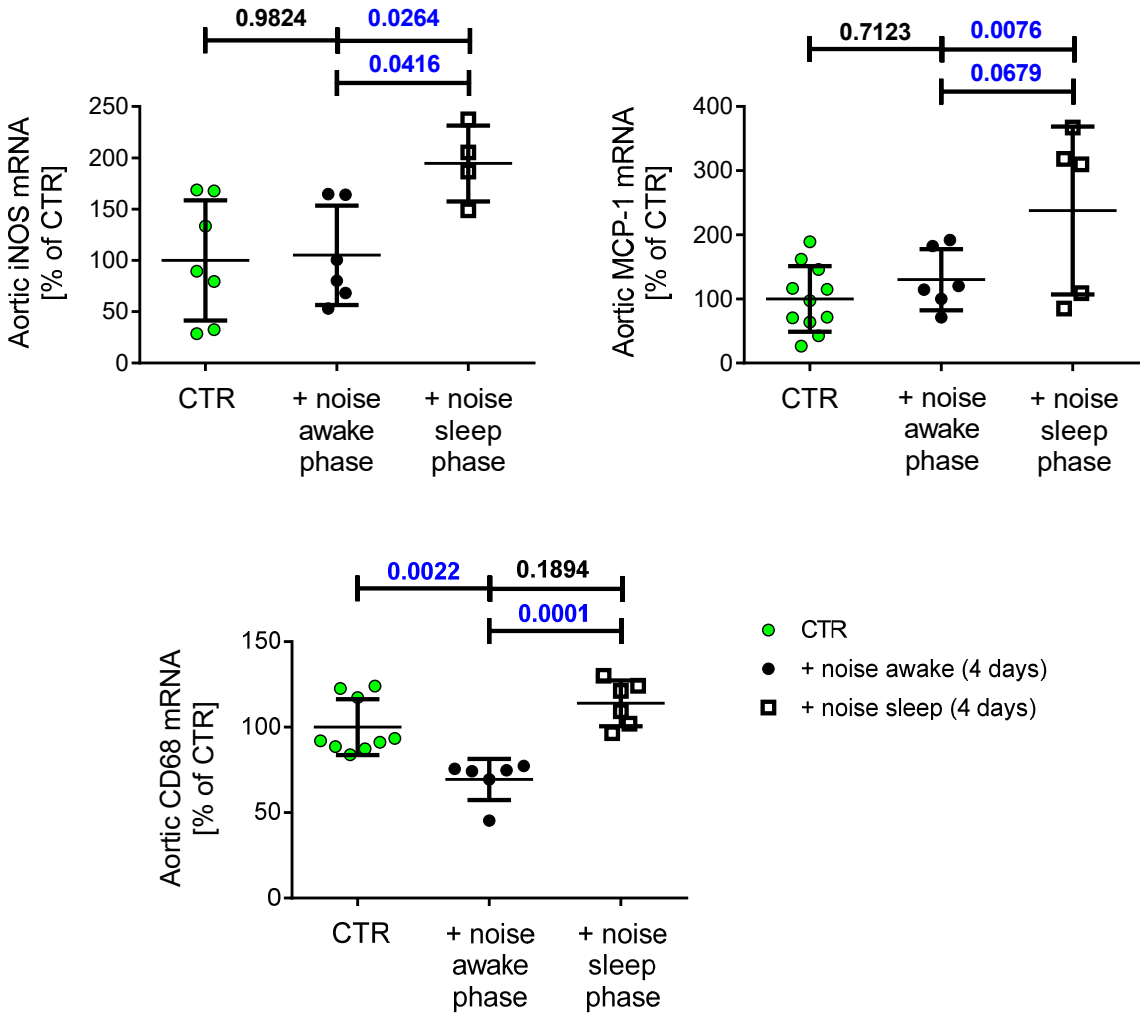

Suppl. Figure S20. Effects of sleep and awake phase noise exposure (12 h/d for 4 d) on vascular markers of inflammation. Levels of inflammation markers in aortic tissue were determined by RT-PCR analysis. mRNA levels of iNOS, MCP-1 and CD68 were increased in the aorta of mice upon noise exposure during the sleep but not the awake phase. Data are mean ± SD from n = 4-11 mice/group. Normality test passed and One-way ANOVA with Tukey's correction was used.

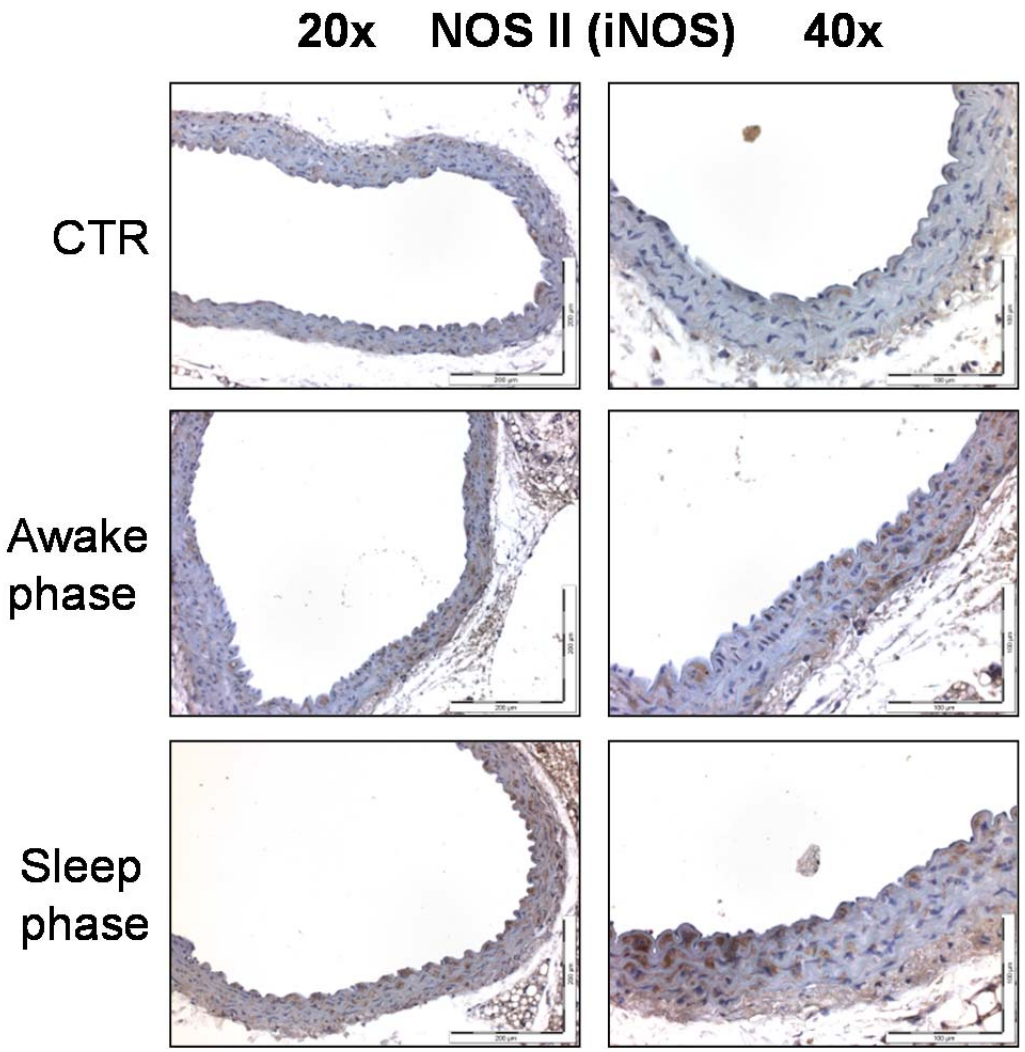

Suppl. Figure S21. Effects of sleep and awake phase noise exposure (12 h/d for 4 d) on vascular iNOS expression. Immunohistochemical analysis revealed that noise exposure during the sleep phase and to a lower extent the awake phase caused an increase in the expression of iNOS in aortic tissue. Representative immunohistochemical images are shown with a magnification of 20x or 40x for at least 3 independent experiments.

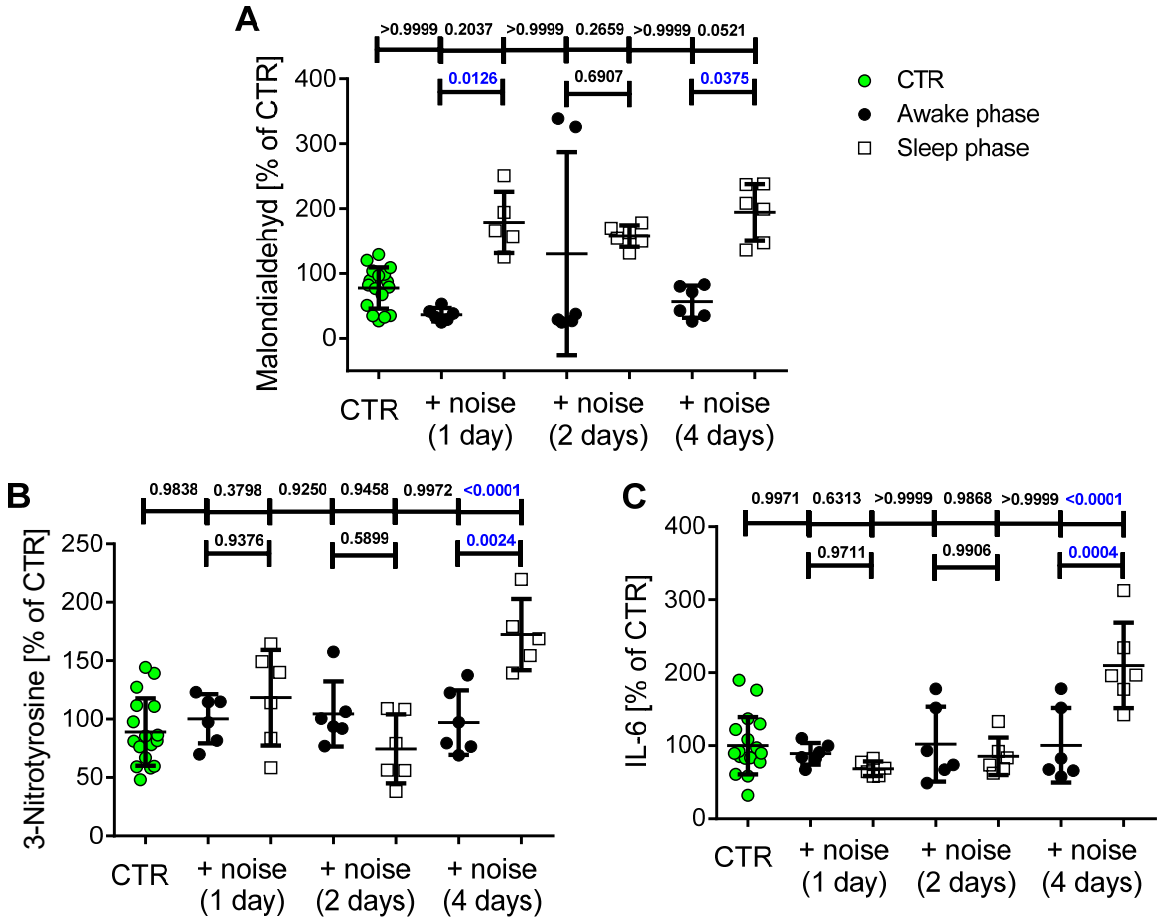

Suppl. Figure S22. Effects of sleep and awake phase noise exposure (12 h/d) on oxidative stress markers (MDA and 3NT) and IL-6 levels in plasma. Levels of malondialdehyde-positive proteins in plasma were significantly elevated in sleep phase noise exposed animals (1 and 4 days, grey bars) but not in awake phase exposure groups (black bars) (**A**). 3-Nitrotyrosine-positive proteins were significantly increased after 4 days of sleep phase noise exposure but not in the awake phase exposure groups (**B**). IL-6 expression in mouse plasma was elevated significantly after 4 days sleep phase noise exposure but not in awake phase noise exposed mice (**C**). Representative dot blots are shown in **suppl. Figure S23**. Data are mean ± SD from 2-3 mouse samples per dot. (**A**) Normality test failed and non-parametric Kruskal-Wallis test with Dunn's correction was used. (**B** and **C**) Normality test passed and One-way ANOVA with Tukey's correction was used.

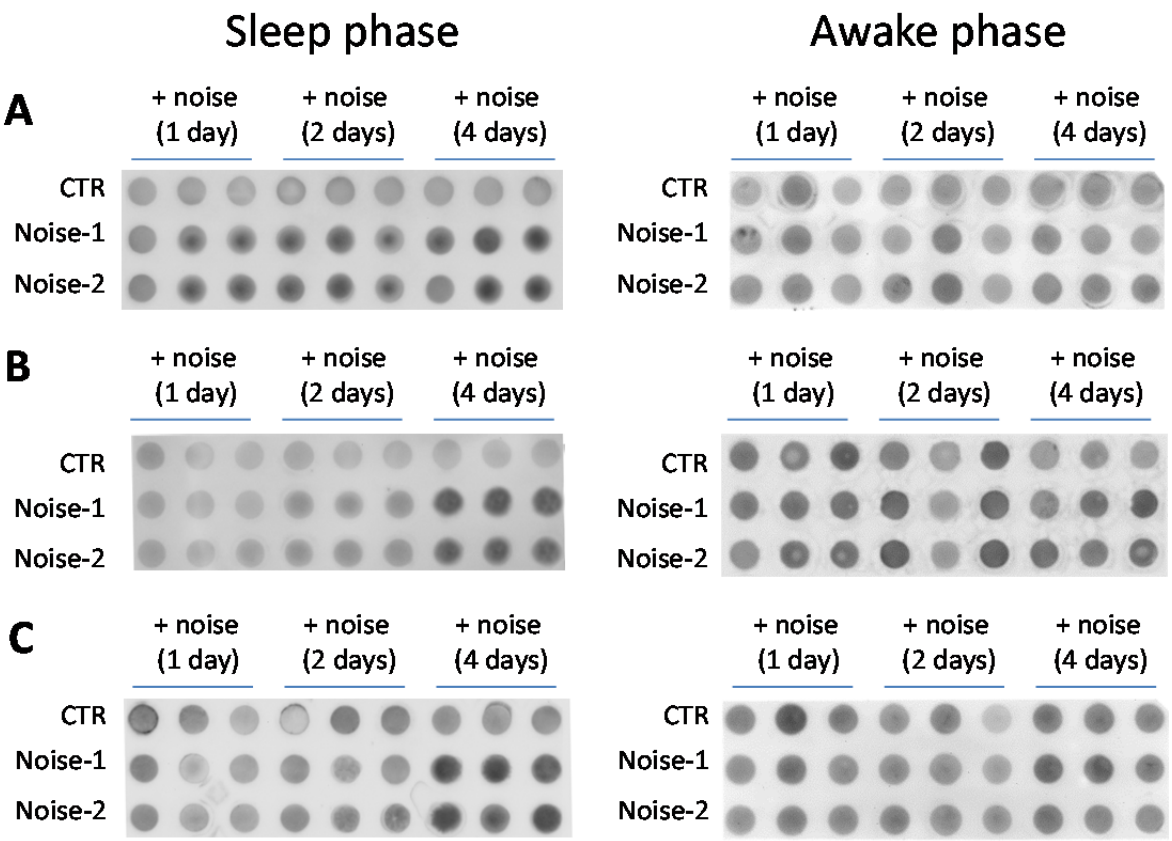

Suppl. Figure S23. Effects of sleep and awake phase noise exposure (12 h/d) on oxidative stress markers (MDA and 3NT) and IL-6 levels in plasma. Representative dot blots are shown for data of **suppl. Figure S22A-C**: malondialdehyde (**A**), 3-nitrotyrosine (**B**) and interleukin-6 (**C**).

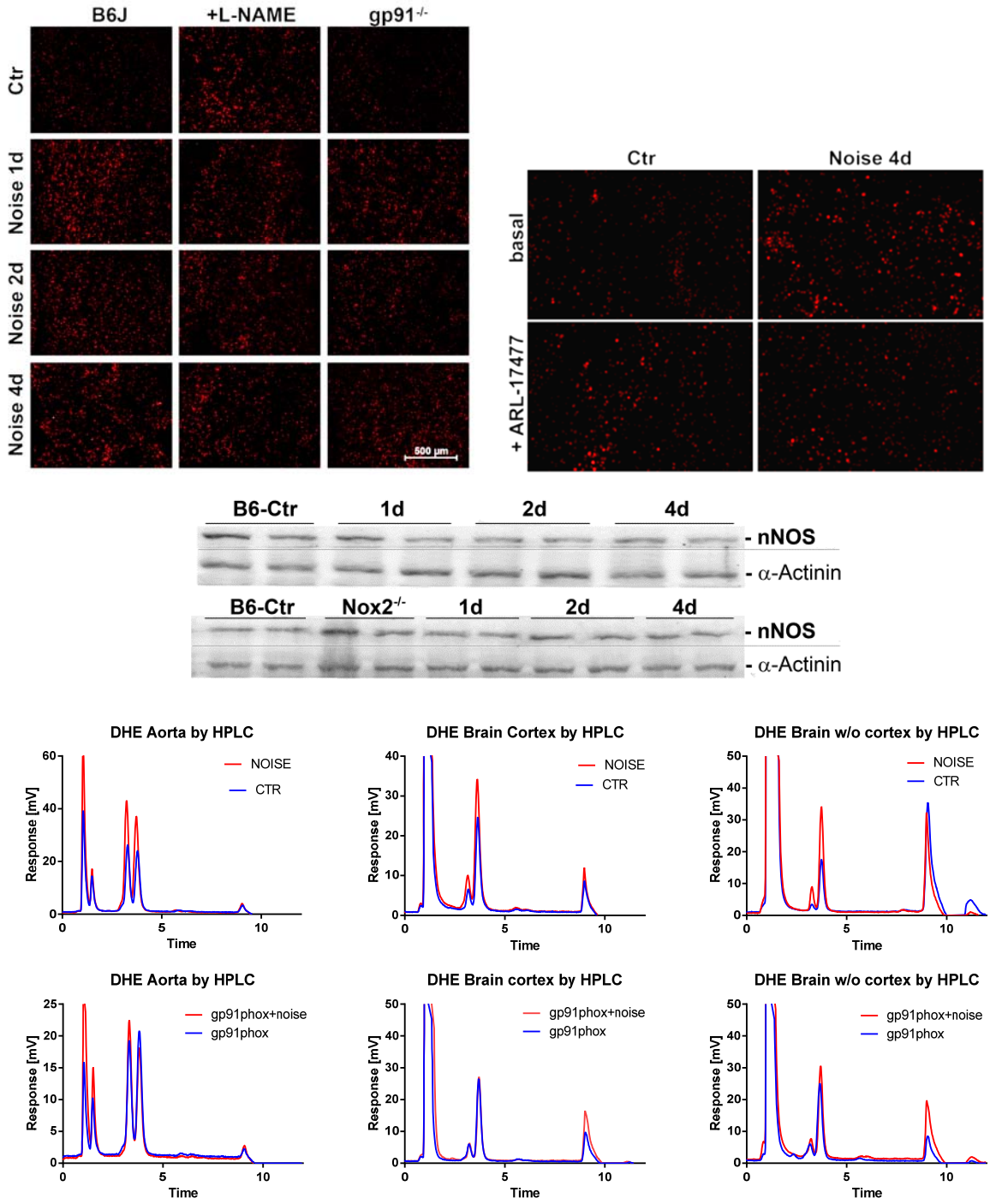

Suppl. Figure S24. Effects of around the clock noise exposure (24 h/d) on vascular and cerebral oxidative stress. Upper panels show the full size representative DHE staining images for the data presented in **Figure 2B** and **2C** in the main manuscript. Middle panel shows the original Western blot for the data presented in **Figure 2D**. Lower panels show the representative HPLC chromatograms for 2-hydoxyethidium data presented in **Figure 1H**, **2F** and **2G** (24h/d noise exposure for 4 d).

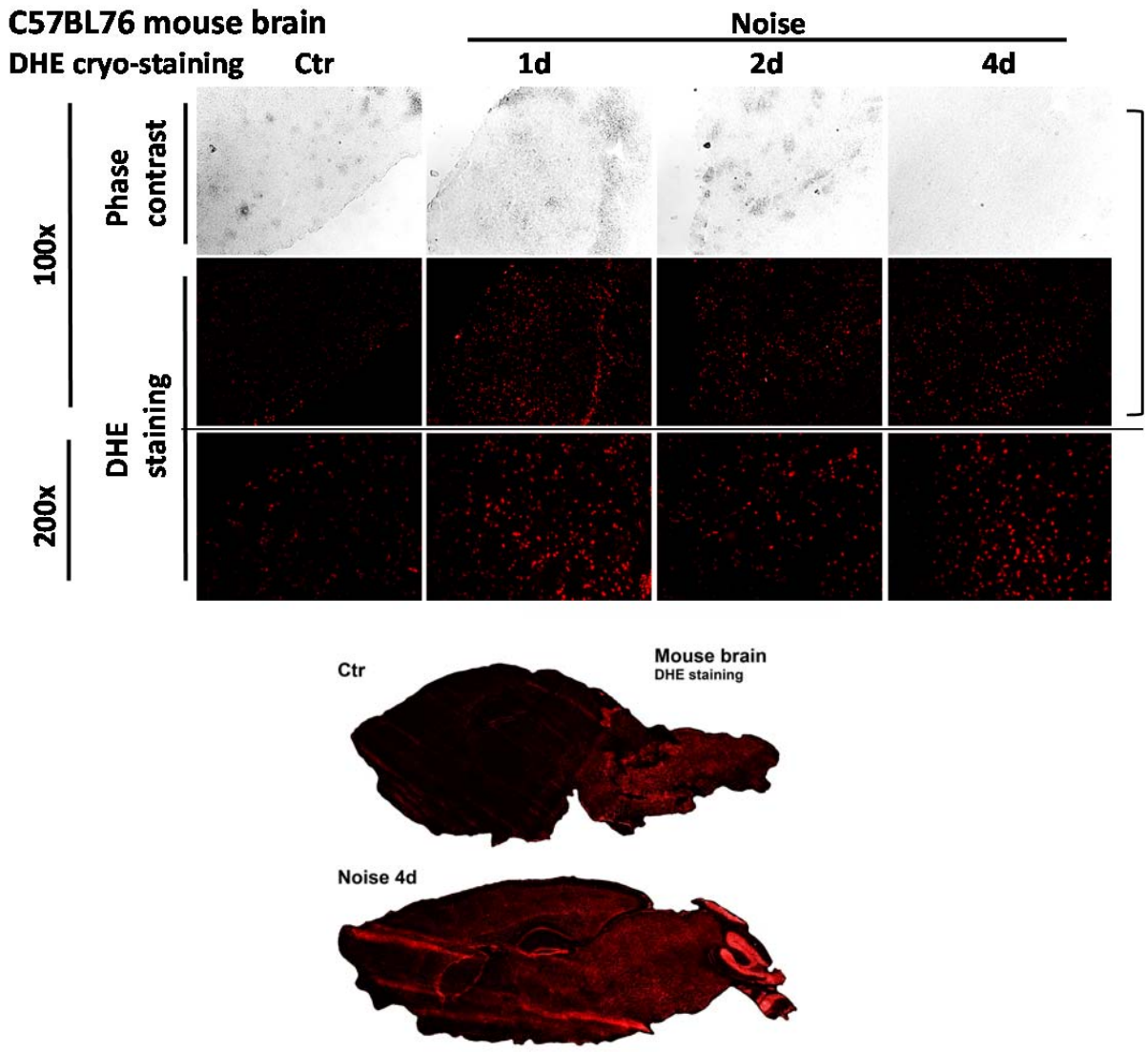

Suppl. Figure S25. Effects of around the clock noise exposure (24 h/d) on cerebral ROS formation. Cryo sections of the frontal cortex were stained with dihydroethidium. Exposure of wild type mice to around the clock aircraft noise induced cerebral ROS formation. Representative pictures to illustrate the procedure of cutting and staining. Lower panel shows DHE staining of total brain sections. Data are representative for at least 3 mice/group. *, $p<0.05$ versus control without noise; #, $p<0.05$ versus WT group on the same day.

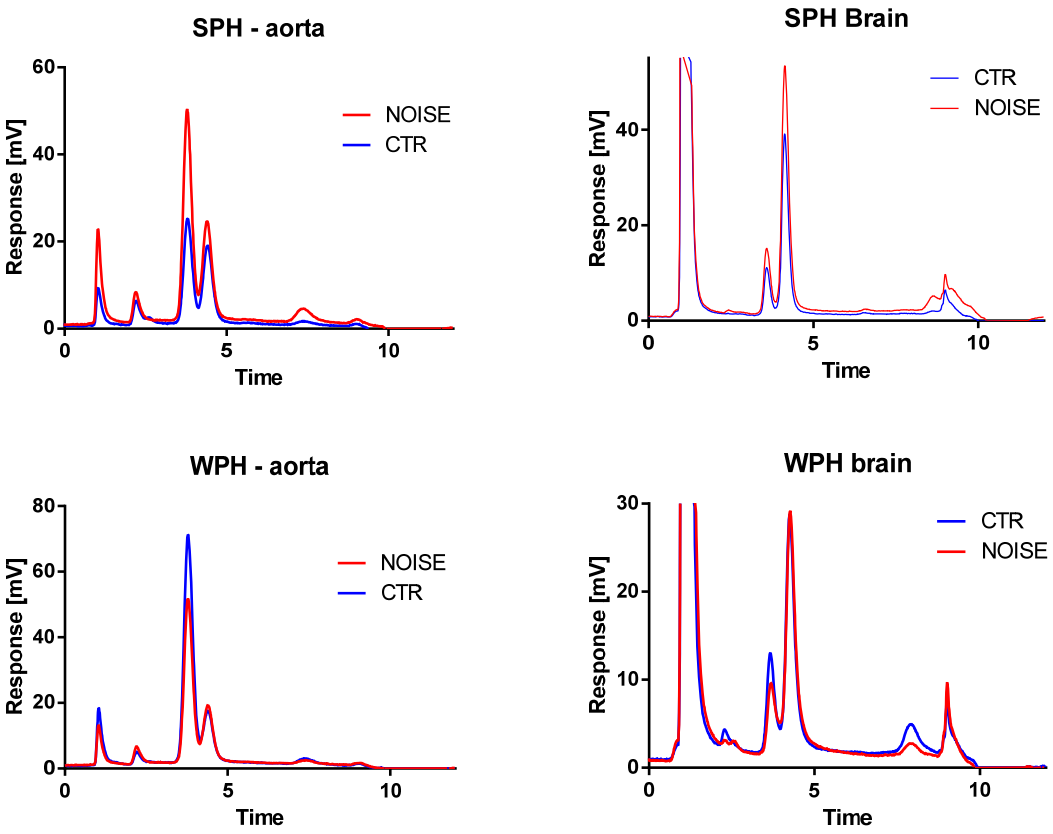

Suppl. Figure S26. Effects of sleep and awake phase noise exposure (12 h/d for 4 d) on vascular and cerebral oxidative stress. Representative HPLC chromatograms for 2-hydoxyethidium data presented in **Figure 4H** and **5B**. SPH, sleep phase; WPH, awake phase.

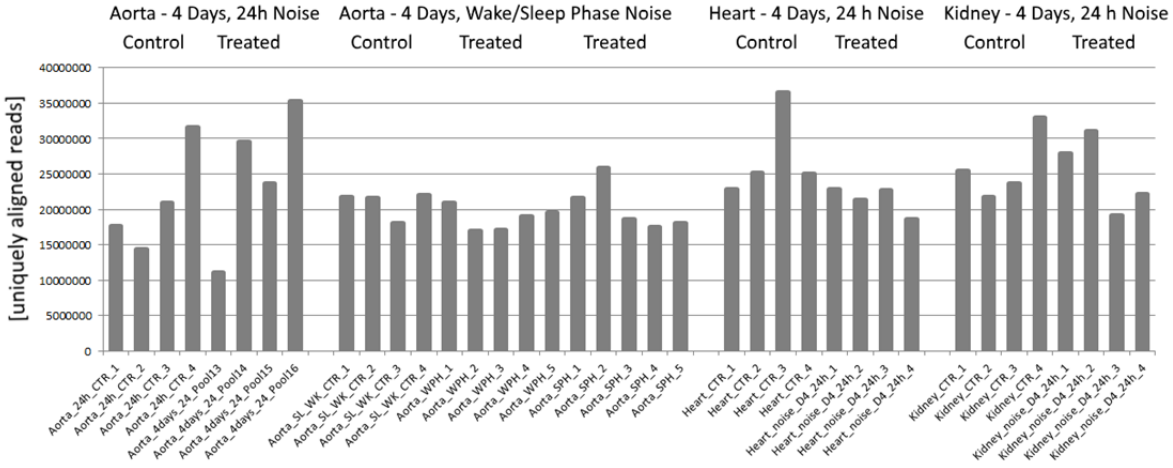

Suppl. Figure S27. Overview of NGS sample pools. The basis for the NGS analyses were a total of 38 sample pools from aorta, heart and kidney (24h noise: 4 Ctr/4 noise for aorta, heart and kidney; 12h noise: 4 Ctr, 5 sleep phase, 5 awake phase). After mapping against human hg19 genome using RESEM/STAR aligner uniquely mapped reads of each pools were reported by DESeq2 and R package pcaExplorer.

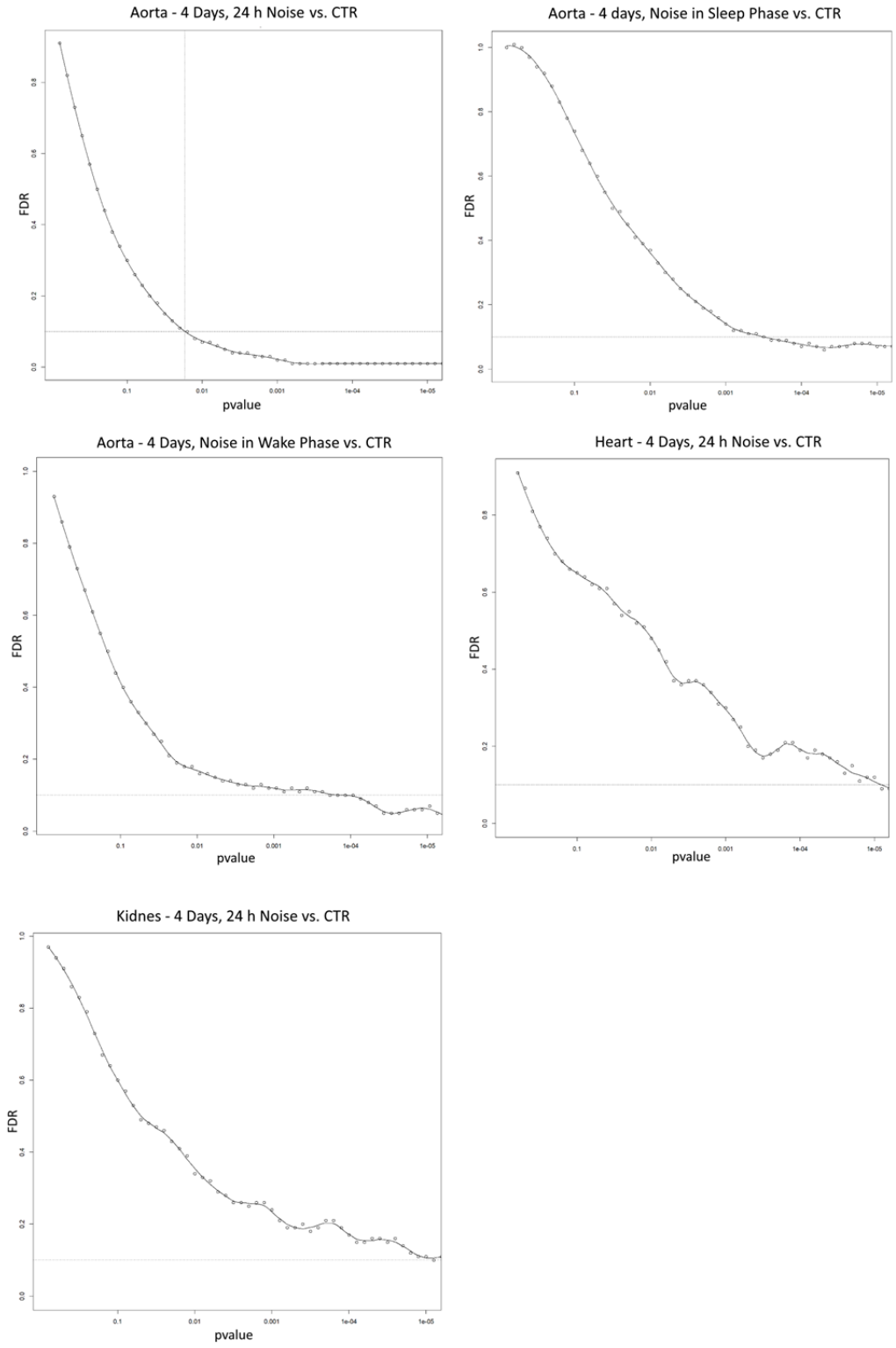

Suppl. Figure S28. Empirical FDR of NGS DEG analysis. Computed und simulated relation between FDR and p-value ("empiricalFDR" R package); according to a FDR of 0.1 the p-value is marked.

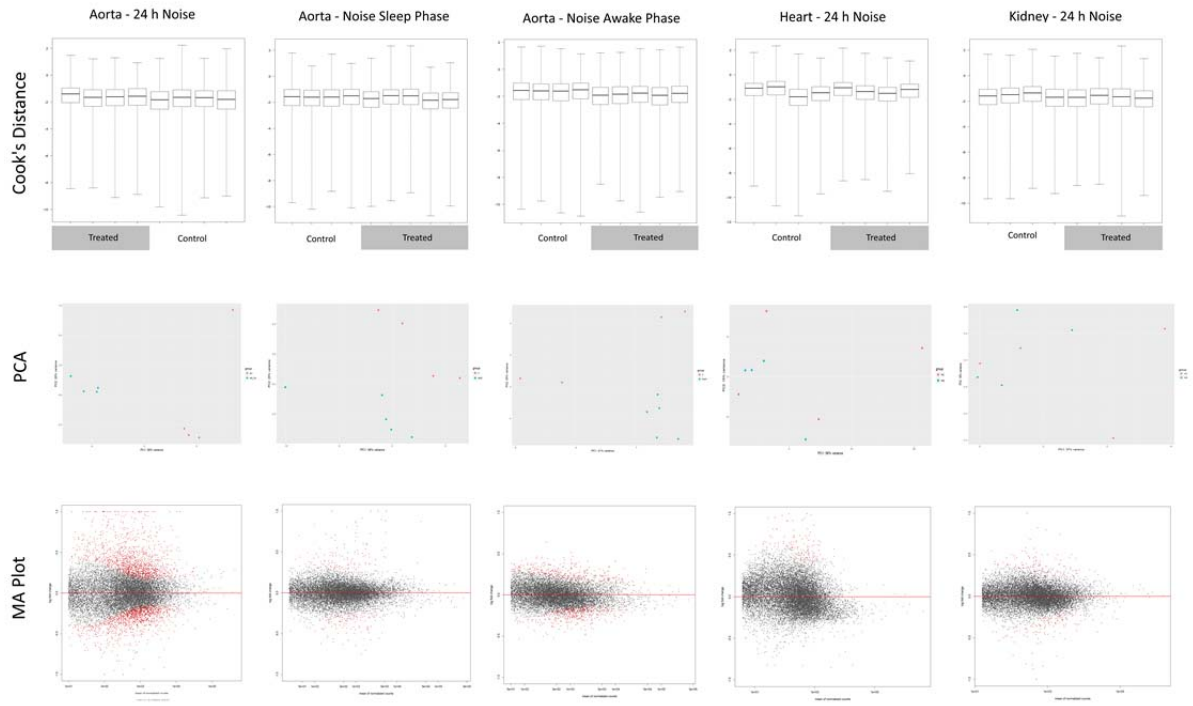

Suppl. Figure S29. Diagnostic plots of NGS DEG analysis. According to possible outliers DESeq2 calculated Cook's distances are shown; "Principal Component Analysis" shows the clustering of sample pools (red dots: controls, blue dots: treated); MA plot shows genes fold change in expression (y) in relation to the mean normalized read counts (x).

Materials and Methods

Noise exposure and other animal treatment

All human data was collected in accordance with the declaration of Helsinki and Ethical approval was granted by the Landesärztekammer Rheinland-Pfalz (Mainz, Germany; permit number: 837.190.12 (8291-F)). Written consent was received from all included individuals. Human data are previously unpublished results of the FLuG-Risiko study [1]. Serum of each individual was sampled after nights without or with aircraft noise exposure for 6 h. The aircraft noise consisted of 60 repetitive noise events, which had been recorded near Düsseldorf airport, interrupted by random silent periods, yielding a mean sound pressure level of 47 dB(A) (compared to 39 dB(A) in the silent nights). The detailed protocol and health status of included individuals was published previously [1].

All animals were treated in accordance with the Guide for the Care and Use of Laboratory Animals as adopted by the U.S. National Institutes of Health and approval was granted by the Ethics Committee of the University Medical Center Mainz and the Landesuntersuchungsamt Rheinland-Pfalz (Koblenz, Germany; permit number: 23 177-07/G 15-1-094). After the indicated duration and protocol of noise exposure (see below), animals were killed under isoflurane anesthesia by transection of the diaphragm and removal of the heart and thoracic aorta. Glucose levels were assessed in whole blood using the ACCU-CHEK Sensor system from Roche Diagnostics GmbH (Mannheim, Germany).

For the continuous 24 h exposure protocol, noise was applied by repetitive playbacks of a 2 h long noise pattern of 69 aircraft noise events with a duration of 43 s and a maximum sound pressure level of 85 dB(A) and an average SPL Leq(3) of 72 dB(A), which does not lead to hearing loss [2]. Noise events were separated by silent periods with irregular distribution to prevent early adaptation. In control experiments, mice were exposed to “white noise” (this is a random noise with constant spectral density within the range of human hearing from 20 Hz to 20 kHz) using exactly the same average SPL as for aircraft noise. For other exposure protocols noise was applied during the inactivity phase (“sleep phase”, 7:00 – 19:00) or activity phase (“awake phase”, 19:00 – 7:00) of the mice for 1, 2 and 4 days. In general mice sleep during the day from 7 am to 7 pm and are awake from 7 pm to 7 am in the morning. The noise pattern was played back from downward facing loudspeakers mounted approximately 30 cm above the mouse cages with a Grundig MS 540 compact sound system with a total output of 65 W. Loudness and corresponding sound pressure levels were calibrated with a Class II Sound level meter (Casella CEL-246) within one the cages at initial setup. Actual SPLs during exposure was continuously recorded during the study period with the same

device placed between cages with upward facing microphone. The average SPL (Leq3) is 72 dB(A) at a usual background noise level of 50 dB(A) in the animal facility. All SPL and maximum sound pressure levels were measured within the mouse cages.

Some noise exposed mice (24 h for 4 d) were treated with bepridil (20 mg/kg/d for 6 d, once daily i.p. injection in DMSO/NaCl 1:1) as reported [3]. The treatment started 2 d prior noise exposure. Mice of the control and noise only groups were treated with the solvent alone.

Isometric tension studies

Perivascular fat was removed from aortas, which were then cut into 4-mm segments. Rings were mounted on force transducers in organ bad chambers, pre-constricted with prostaglandin $F_{2\alpha}$ (yielding approximately 80 % of the maximal tone induced by KCl bolus) and concentration-relaxation curves in response to increasing concentrations of acetylcholine (ACh) and nitroglycerin (GTN) were performed as described [4, 5].

ELISA for leptin, 3-nitrotyrosine and 8-isoprostane

Circulating leptin was determined in mouse serum using a commercial enzyme-linked immunosorbent assay (ELISA) kit (mouse/rat leptin immunoassay, #MOB00, R&D Systems) following the instructions of the vendor. Levels of 3-nitrotyrosine and 8-isoprostane were determined in human serum using a commercial enzyme-linked immunosorbent assay (ELISA) kit (human immunoassay, 3NT: #CSB-E14324h, Cusabio, Wuhan, Hubei Province 430206, China; 8IP: #MBS109360, San Diego, CA, USA) following the instructions of the vendor.

Immunohistochemical staining of aortic rings and brain

First aortic segments were fixed in paraformaldehyd (4%) and paraffin-embedded. Paraffin-embedded aortic samples were stained with a primary antibody against ET-1 as described [6]. ET-1 staining was performed using a specific antibody (Pierce #MA3-005: 1:200). A biotinylated secondary antibody (Thermo Fisher Scientific, Waltham, MA) was used at a dilution according to the manufacturer's instructions. Sections were stained for iNOS made in rabbit (#N20 sc-651, Santa Cruz, Dallas) diluted 1:50 in Antibody Diluent (DAKO #S0809, Agilent, Santa Clara, CA). The biotinylated secondary antibody (Thermo Fisher Scientific, Waltham, MA) was used at a dilution 1:1,100. For immunochemical detection ABC reagent (Vector) and then DAB reagent (peroxidase substrate Kit, Vector)

were used as substrates. Quantification was performed using Image ProPlus 7.0 software (Media Cybernetics, Rockville, MD).

Immunohistochemical stainings for detection of astrocytes and microglia were performed using standard methods as described [7, 8]. In brief, slices were dewaxed through graded alcohols. Sections were then incubated in Ventana buffer, and automatically stained with the NEXEX immunohistochemistry robot (Ventana Instruments) using primary antibodies GFAP (1:300; polyclonal, rabbit, DAKO, Glostrup for astrocytes and Iba-1 (1:1,000; polyclonal, rabbit, Wako, Osaka, Japan) for microglia. Finally, sections were developed using an iVIEW DAB Detection Kit (Ventana). Omission of the primary antisera in a subset of control slides resulted in no immunostaining at all. Sections were scanned under equal lighting conditions at 40x magnification using a Hamamatsu tissue scanner (Nanozoomer). Hamamatsu NDPI images of each scanned slide were transferred to a computer screen (Viewer Version DIH 4.0.0-20130402-63) and were investigated by a neuropathologist for astrogliosis and microglia activation. Finally, representative images (jpeg) from the area of the hippocampus region CA1 with adjacent corpus callosum (CC) were captured.

Detection of oxidative stress and inflammation in plasma, cardiac tissue, brain and aorta

Vascular ROS formation was determined using dihydroethidium (DHE, 1 μM)-dependent fluorescence microtopography in aortic cryo-sections as described [9, 10] or in brain sections of the frontal cortex (see also **suppl. Figure S25**). To investigate the involvement of eNOS uncoupling in ROS production and endothelial dysfunction, aortic rings were preincubated with the NOS inhibitor L-NAME (0.5 mM) and red fluorescence of DHE oxidation products was only quantified in the endothelial cell layer [9-11]. In order to test for nNOS uncoupling the cryo sections were preincubated for 20 min with the highly specific nNOS inhibitor ARL-17477 (1 μM). In order to test for Nox activity the cryo sections were preincubated for 20 min with the Nox2 inhibitor GSK2795039 (50 μM), which also inhibits other Nox isoform at higher concentrations [12]. Likewise, mitochondrial ROS formation was determined using mitochondria-targeted dihydroethidium (mitoSOX, 1 μM)-dependent fluorescence microtopography in brain cryo-sections as described [13]. ROS-derived red fluorescence was detected using a Zeiss Axiovert 40 CFL microscope, Zeiss lenses and Axiocam MRm camera.

Protein tyrosine nitration was detected using a specific antibody for 3-nitrotyrosine (3NT, 1:1,000, Upstate Biotechnology, MA, USA) and lipid peroxidation using a specific

antibody for malondialdehyde (MDA)-positive proteins (1:1,000, Calbiochem, Darmstadt, Germany) in EDTA plasma. Inflammation was detected using a specific antibody for interleukin-6 (anti IL-6 rabbit antibody, abcam, ab6672) in EDTA plasma. Briefly, 100 µl (0.5 µg/µl protein based on Bradford analysis) of the EDTA plasma were transferred to a Protran BA85 (0.45 µm) nitrocellulose membrane (Schleicher&Schuell, Dassel, Germany) by a Minifold I vacuum Dot-Blot system (Schleicher&Schuell, Dassel, Germany). Each slot was washed twice with 200 µl PBS before and after protein transfer. The membrane was dried for 60 min at 60 °C. Positive bands were detected by enhanced chemiluminescence after incubation with a peroxidase-coupled secondary antibody (GAM-POX and GAR-POX, 1:10,000) (Vector Laboratories, CA, USA). All incubation and washing steps were performed according to the manufacturer's instructions. Densitometric quantification of the dots was performed using the Super Signal ECL kit from Thermo Scientific.

For simultaneous detection of 45 human cytokines and chemokines (see list below), we used the BioPlex Pro™ human ProcartaPlex assay (96-well). The assay kit was purchased from Thermo Fisher Scientific (#EPX450-12171-901, Darmstadt, Germany). The serum samples were collected in a standard serum monovette and were used without dilution. The assay was performed according to the instructions of the manufacturer and as previously published [14]. For the washing steps, we used a hand-hold-magnet (Invitrogen). Samples were analyzed on the Luminex xMAP™/Bioplex-200 System with BioPlex Manager™ Software 6.1. We only obtained data for 32 cytokines / chemokines (13 targets showed no signal at all), 24 of them showed no difference and of the remaining 8 targets 6 datasets contained only two values in one of the groups. Data for the remaining two cytokines are shown in the main manuscript (**Figure 6**).

Target List
BDNF; Eotaxin/CCL11; EGF; FGF-2; GM-CSF; GRO alpha/CXCL1; HGF; NGF beta; LIF; IFN alpha; IFN gamma; IL-1 beta; IL-1 alpha; IL-1RA; IL-2; IL-4; IL-5; IL-6; IL-7; IL-8/CXCL8; IL-9; IL-10; IL-12 p70; IL-13; IL-15; IL-17A; IL-18; IL-21; IL-22; IL-23; IL-27; IL-31; IP-10/CXCL10; MCP-1/CCL2; MIP-1 alpha/CCL3; MIP-1 beta/CCL4; RANTES/CCL5; SDF-1 alpha/CXCL12; TNF alpha; TNF beta/LTA; PDGF-BB; PLGF; SCF; VEGF-A; VEGF-D
Bead Regions
IFN gamma: 43; IL-12p70: 34 ; IL-13: 35; IL-1 beta: 18; IL-2: 19; IL-4: 20; IL-5: 21; IL-6: 25; TNF alpha: 45; GM-CSF: 44; IL-18: 66; IL-10: 28; IL-17A: 36; IL-21: 72; IL-22: 76; IL-

23: 63; IL-27: 14; IL-9: 52; IFN alpha: 48; IL-31: 37; IL-15: 65; IL-1 alpha: 62; IL-1RA: 38; IL-7: 26; TNF beta: 54; Eotaxin: 33; GRO alpha: 61; IL-8: 27; IP-10: 22; MCP-1: 51; MIP-1 alpha: 12; MIP-1 beta: 47; RANTES: 42; SDF-1 alpha: 13; NGF beta: 55; EGF: 56; FGF-2: 75; HGF: 46; BDNF: 57; PDGF-BB: 77; PIGF-1: 29; SCF: 39; VEGF-A: 78; LIF: 15; VEGF-D: 53

Leukocyte-dependent oxidative burst is a read-out for leukocyte-dependent hydrogen peroxide formation (mainly by phagocyte-type NADPH oxidase, Nox2). Hydrogen peroxide is converted by myeloperoxidase to highly reactive oxygen-metal complexes that lead to oxidation of L-012 to an intermediate that by chemical reaction emits energy in the form of chemiluminescent light. Oxidative burst was measured in fresh citrate blood upon dilution 1:50 and stimulation with zymosan A (50 µg/ml) as well as phorbol ester dibutyrate (10 µM) in PBS buffer containing Ca^{2+}/Mg^{2+} (1 mM) by L-012 (100 µM) enhanced chemiluminescence (ECL) using a Mithras2 chemiluminescence plate reader (Berthold Technologies, Bad Wildbad, Germany) [6, 15]. L-012 (8-amino-5-chloro-7-phenylpyrido[3,4-d]pyridazine-1,4-(2H,3H)dione sodium salt) was purchased from Wako Pure Chemical Industries (Osaka, Japan).

Oxidative stress and superoxide was also measured by a modified HPLC-based method to quantify 2-hydroxyethidium levels as previously described [10, 16]. Briefly, tissue of aorta, whole brain or frontal cortex was incubated with 50 µM DHE for 30 min at 37 °C in PBS buffer. Tissues were snap-frozen and stored at -80 °C until they were homogenized in 50 % acetonitrile/ 50 % PBS (brain, frontal cortex) or pulverized in a mortar under liquid nitrogen and resuspended in homogenization buffer (aorta), centrifuged and 50 µl of the supernatant were subjected to HPLC analysis. The system consisted of a control unit, two pumps, mixer, detectors, column oven, degasser and an autosampler (AS-2057 plus) from Jasco (Groß-Umstadt, Germany) and a C_{18}-Nucleosil 100-3 (125x4) column from Macherey & Nagel (Düren, Germany). A high pressure gradient was employed with acetonitrile and 50 mM citrate buffer pH 2.2 as mobile phases with the following percentages of the organic solvent: 0 min, 36 %; 7 min, 40 %; 8-12 min, 95 %; 13 min, 36 %. The flow was 1 ml/min and DHE was detected by its absorption at 355 nm whereas 2-hydroxyethidium were detected by fluorescence (Ex. 480 nm/Em. 580 nm).

S-glutathionylation of endothelial nitric oxide synthase and Ser847 phosphorylation of neuronal nitric oxide synthase by immunoprecipitation

Immunoprecipitation of aortic endothelial NO synthase (eNOS) or brain neuronal NO synthase (nNOS) and subsequent immunoblotting of the precipitate for S-glutathionylation or nNOS-Ser847 phosphorylation was performed according to a standard protocol as recently published [17]. M-280 sheep anti-mouse IgG coated beads from Invitrogen (Darmstadt, Germany) were used along with a monoclonal mouse eNOS (BD Biosciences, USA) or a monoclonal mouse nNOS antibody (BD Biosciences, USA). The beads were loaded with the eNOS or nNOS antibody and cross-linked according to the manufacturer's instructions. Next, aortic homogenates were incubated with the eNOS antibody beads and brain homogenates were incubated with the nNOS antibody beads, respectively. After precipitation with a magnet, the samples were washed and transferred to the gel and subjected to SDS-PAGE followed by a standard Western blot procedure using a monoclonal mouse antibody against S-glutathionylated proteins from Virogen (Watertown, MA, USA) at a dilution of 1:1,000 under non-reducing conditions for eNOS precipitates and for nNOS precipitates against nNOS-Ser847 phosphorylation from abcam (rabbit polyclonal antibody, Cambridge, UK) at a dilution of 1µg/ml. After stripping of the membrane, the bands were immunoblotted for eNOS (mouse monoclonal, 1:1,000, BD Biosciences, USA) or for nNOS (mouse monoclonal, 1:500, BD Biosciences, USA) to allow normalization of the signals. Detection and quantification were performed by enhanced chemiluminescence (ECL) with peroxidase conjugated anti–mouse/rabbit (GAM-POX/GAR-POX, 1:10,000, Vector Lab., Burlingame, CA) secondary antibodies. Densitometric quantification of antibody-specific bands was performed with a ChemiLux Imager (CsX-1400M, Intas, Göttingen, Germany) and Gel-Pro Analyzer software (Media Cybernetics, Bethesda, MD).

Western Blotting Analysis of Other Proteins

The procedures were similar to those described recently [18]. Aortic protein samples were analyzed by Western blot analysis for endothelial NO-synthase (eNOS, mouse monoclonal, 1:1,000, BD Biosciences, USA), phospho-Ser1177-eNOS (rabbit polyclonal, 1:1,000, Cell Signaling, Danvers, MA, USA), dihydrofolate reductase (DHFR, mouse monoclonal, 1 µg/ml, Abnova Corp., Germany), GTP-cyclohydrolase-1 (GCH-1, mouse monoclonal, 1 µg/ml, Abnova Corp., Germany), cGMP-dependent protein kinase (cGK-1, goat polyclonal, 1:200, SantaCruz, Dallas, USA), Ser239 phosphorylated vasodilator-stimulated phosphoprotein (P-VASP, clone 16C2, 1.5 µg/ml, Calbiochem, UK), endothelin-1 (ET-1, rabbit polyclonal, 1:5,000, Abcam, Cambridge, MA, USA), monoclonal mouse heme oxygenase-1 (HO-1) (4 µg/ml, Stressgen, San Diego, CA) and monoclonal mouse α-actinin or

polyclonal rabbit β-actin (both 1:2,500, Sigma-Aldrich) for normalization of loading and transfer. For quantification of expression or phosphorylation of protein in brain homogenate (whole brain and/or frontal cortex) a monoclonal nNOS antibody (1:500, BD Bioscience, USA), antibodies against NADPH oxidase subunits Nox1 (rabbit polyclonal, 1:500, Abcam, Cambridge, MA, USA), Nox2 (mouse monoclonal $gp91^{phox}$, 1:1000, BD Biosciences, USA), Nox3 (rabbit polyclonal, 1:1000, Novus biologicals, Abingdon, UK), Nox4 (rabbit polyclonal, 1:500, Abcam, Cambridge, MA, USA), p47Phox (rabbit polyclonal, 1:1000, Upstate Biotechnology, MA, USA) and phosphorylated p47Phox at serin 328 (rabbit polyclonal P-47Phox (Neutrophil Cytosolic Factor 1, NCF1 pS328), 1:500, Assay Biotech, Fremont, CA, USA), a monoclonal protein kinase C beta subunit antibody (PKC_{β}, 1:250, BD Bioscience, USA), a polyclonal Phospho-MARCKS antibody (Myristorylated alanine-rich protein kinase C substrate phosphorylated at serin 152/156, 1:1000, Cell Signaling, Danvers, MA, USA), a polyclonal MCP-1 antibody (monocyte chemotactic protein-1, 1:500, Bio-Rad Laboratories GmbH, Germany) and a polyclonal MyD88 antibody (myeloid differentiation factor 88, 1:1000, Cell Signaling, Danvers, MA, USA) was used. Secondary antibodies (GAM-POX, GAR-POX (see above) or donkey anti goat-peroxidase labeled, 1:5,000, Santa Cruz, USA) and ECL development as described above for dot blot.

Quantitative reverse transcription real-time PCR (qRT-PCR)

Total mRNA from aortic tissue was isolated using the RNeasy Fibrous Tissue Mini Kit, Qiagen, Hilden, Germany according to the manufacturers protocol. 50 ng of total RNA was used for quantitative reverse transcription real-time PCR (qRT-PCR) analysis using QuantiTect Probe RT-PCR kit (Qiagen) as described previously [6, 19]. Primer-Probe-Mixes purchased from Applied Biosystems, Foster City, CA were used to analyze the mRNA expression patterns of *indian hedge hog protein* (*Ihh*, Mm00439613_m1), *aryl hydrocarbon receptor nuclear translocator-like protein 1* (*Arntl*, Mm00500226_m1), *inducible NO-synthase* (*Nos2*, Mm00440485_m1), *vascular cell adhesion molecule 1* (*Vcam1*, Mm00449197_m1), *poly[ADP-ribose]polymerase 1* (*Parp1*, Mm01321084_m1), *monocyte chemoattractant protein 1* (*Mcp1*, Mm_00441242_m1), *cluster of differentiation 68* (*CD68*, Mm_00839636_g1) and *Forkhead-Box-Protein O3* (*Foxo3*, Mm01185722_m1) normalized on the *TATA box binding protein* (*TBP*, Mm_00446973_m1) as an internal control. In brain tissue a primer-probe-mix was used to analyze mRNA of *neuronal nitric oxide synthase* (*Nos1*, Mm01208059_m1), *interleukin-6* (*IL-6*, Mm_00446190_m1), *catalase* (*Cat*, Mm_00437992_m1) and *NADPH oxidase 1* (*Nox1*, Mm_01340623_m1). For quantification

of the relative mRNA expression the comparative ΔΔCt method was used. Gene expression of target gene in each sample was expressed as the percentage of wildtype.

Non-invasive blood pressure measurements (NIBP)

NIBP measurements were performed on a daily basis throughout the noise exposure regimen (CODA 2, Kent Scientific, Torrington, USA). Animals were placed in restraining tubes on a preheated plate (32 °C). The CODA System relies on two tail-cuffs to measure blood pressure. An occlusion cuff and a volume-pressure recording cuff are positioned on the tail. Data have been acquired by CODA data Acquisition Software. Five measurements were performed in advance to get the animal used to it. The mean values of ten NIBP readings were used for each animal. Feng et al. proofed accuracy of this method compared to radiotelemetric measurement [20].

Next generation sequencing

RNA extraction. To investigate gene expression changes in mouse aorta, heart, kidney and brain tissue after noise exposure four sample pools of each condition were analyzed (n=4 samples per tissue for 24h noise exposure; n=4-5 aortic samples for sleep/awake noise exposure; 38 pools in total). Each pool consisted of tissue from four animals. As described in detail [18], tissue pools were used for RNA extraction (PEQLab precellys™, VWR, Darmstadt, Germany), concentration and quality were assessed with a Bioanalyzer 2100 (Agilent RNA Nano or Pico chips Agilent Technologies, Santa Clara, USA) and 0.5 – 1.0 µg of total RNA of each pool were used for sequencing library preparation (TruSeq Stranded mRNA™, Illumina, San Diego, USA).

Illumina sequencing. For aortic tissue the sequencing of the cDNA sequencing libraries of aortic tissue after 4 days noise treatment was carried out as 150 bp paired-end runs on an Illumina NexSeq500™ (Illumina, San Diego, USA) by StarSEQ GmbH (Mainz, Germany) followed by quality trimming and removing adapter sequences. The sequencing of the cDNA sequencing libraries of aorta after noise treatment in sleep and wake phase for 4 days as well as from heart, kidney and brain (around-the-clock noise exposure for 4d) was carried out as 50 bp single read runs on an Illumina HiSeq2500™ (Illumina, San Diego, USA) at the Institute of Molecular Genetics (JGU, Mainz, Germany) followed by quality trimming and removing adapter sequences.

Analysis of Illumina RNA-Seq data. For RNA-Seq analysis paired end reads were mapped against UCSC mouse genome build GRCm38/mm10 (Dec. 2011) using STAR [21] combined with the RSEM [22] data analyzing pipeline with the default settings. Results were processed in R [23] (Version 3.3.1 and 3.3.2) using DESeq2 [24] package for calling differential gene expression. As part of the DESeq2 package p-values were adjusted by Benjamini & Hochberg correction to control for false positives. For data quality overview see **suppl. Figure S27** and **S28**. Threshold for significant expression changes was set to padj < 0.05. The "empiricalFDR.DESeq2" (M. V. Matz, 2015) R package was used to simulate read counts according to the null hypothesis and to compute the empirical false discovery rate (see **suppl. Figure S29**). Gene sets with significant changes ($p < 0.05$) were mapped to selected KEGG [25, 26] pathways using Pathview [27] package. Mappings and generation of pathway figures were done with default settings. Expression values (FPKM) of genes involved in pathways of particular interest were extracted without consideration of DESeq2 generated p-values. Significance of expression changes compared to the untreated controls was checked by one-way ANOVA with Bonferroni's correction (Prism for Windows, version 7.01, GraphPad Software Inc.). Pathway networks were extended by literature search and GIANT [28] database search.

Heat maps were generated using GraphPad Prism 6 software. Pie graphs were generated using the free online software Venny 2.0.

Statistical analysis

Results are expressed as the means ± SD. Two-way ANOVA (with Bonferroni's correction for comparison of multiple means) was used for comparisons of concentration-relaxation curves (Prism for Windows, version 7.01, GraphPad Software Inc.). One-way ANOVA (with Bonferroni's correction for comparison of multiple means) or, where appropriate, equivalent non-parametric Kruskal-Wallis test (Dunn multiple comparison) was used for comparisons of blood glucose, other serum/plasma parameters, 3NT, MDA, histological data, aortic and brain ROS formation, protein and mRNA expression, blood pressure (SigmaStat for Windows, version 3.5, Systat Software Inc.). For the human crossover study samples (18 matched pairs before and after noise exposure) the "Wilcoxon matched-pairs signed rank test" was used for statistical analysis of 3-nitrotyrosine and 8-isoprostane (all data paired), whereas the unpaired t-test (without and with Welch's correction) was used for statistical analysis of interleukin-1β and -18 (not all data paired) (Prism for Windows, version 7.01, GraphPad Software Inc.). p-values < 0.05 were considered

as statistically significant and absolute p-values are provided in the figures. The number of replicates in the different assays may vary since not all animals were used in all assays.

Statistical sample size calculation

An a priori power analysis was performed to estimate the numbers of mice needed for significant results. Differences in flow mediated dilation measured in an human aircraft noise study were used as calculation basis [1]. Following input parameters were used for the computation of sample size effect size = 0.8, alpha = 0.05, Power (1-beta) = 0.95. The analysis was performed for an one tailed parametric test between two groups with independent means with the freely available G*Power Software [29]. An overall sample size of n = 70 (with Df = 68) with equal group allocation was calculated. All animal experiments planning were guided by this initial sample size estimation, which helped preventing unnecessary test animal breeding and loss.

[40] -- *Thursday, December 08, 2016 -- 18:02:01*

t tests - Means: Difference between two independent means (two groups)

Analysis:	A priori: Compute required sample size		
Input:	Tail(s)	=	One
	Effect size d	=	0.8
	α err prob	=	0.05
	Power (1-β err prob)	=	0.95
	Allocation ratio N2/N1	=	1
Output:	Noncentrality parameter δ	=	3.3466401
	Critical t	=	1.6675723
	Df	=	68
	Sample size group 1	=	35
	Sample size group 2	=	35
	Total sample size	=	70
	Actual power	=	0.9523628

Extended Discussion

Noise exposure is an environmental stressor with severe effects on the brain and metabolism

From the pathophysiological point of view, noise can be considered as a non-specific stressor that causes disturbance of sleep and emotional responses such as annoyance when applied during the daytime due to impairment of communication and activity. This is characterized by an activation of the sympathetic nervous system and exacerbates cardiovascular risk factors including increases in blood pressure and dyslipidemia, increased blood viscosity and blood glucose levels and an activation of blood clotting factors (for review see[30]). It is also well established that severe life stress (including sleep deprivation) triggers cerebral oxidative stress, followed by neuronal inflammation and activation of the angiotensin-II pathway in the brain with a secondary activation of NADPH oxidase (mainly the phagocyte-type NADPH oxidase [Nox2]), microvascular and neuronal inflammation[31]. Increased levels of angiotensin-II and cortisol are also adverse features observed upon chronic noise exposure in animals[18, 32] and human subjects[33]. Likewise, large-scale population-based cohort studies identified that noise exposure during pregnancy and childhood increased the risk of overweight at 7 years of age (40,974 individuals)[34] and in exposed adults as well (57,053 individuals)[35].

Effects of around-the-clock, sleep and awake phase aircraft noise on circadian clock regulating genes

In our previous study, we found that continuous aircraft noise exposure significantly altered expression of genes involved in important cellular processes involving apoptosis, cell growth, fibrosis, inflammation and antioxidant defense [18]. The 8 most significantly up- or downregulated genes encode for transcription factors, proteins with nuclear localization, key phosphatases or regulators of autophagy, calcium signaling and responses to hypoxia (*Zbtb44, Setad4, Ypel2*, *Ihh*, *Sacs, Nbeal1, Ptpn4* and *NR4A3*). An appreciable part of the regulated genes was found to be involved in essential cellular pathways such as TGFβ, Smad, NFκB related and FOXO signaling [18]. Of note, FOXO and NFκB activity are largely redox-regulated processes [36-40].

Our present extension of these previous NGS data reveal a potential link between *Foxo3* expression / activity and important genes of the circadian clock system (**suppl. Tables S1-S3, Figure 1 and suppl. Figure S5**), which may be directly activated by increased nitrosative stress or alterations of protein phosphatases and calcium signaling [41-44]. A role for *Foxo3* in the circadian clock is in accordance to previous reports demonstrating that circadian

clock oscillation is irregular and the period is variable upon deletion of *Foxo3* [45]. Disruption of the circadian clock provides an attractive explanation for the adverse effects of around-the-clock noise exposure as observed in the present studies e.g. due to sleep deprivation and fragmentation. As mentioned in the introduction, sleep deprivation and fragmentation causes cerebral oxidative stress by activation of the hypothalamic–pituitary–adrenal (HPA) axis and cortisol production [46-48], and specifically Nox2 was recently identified to play an important role for learning and memory impairment [49]. Vice versa, a significant impact of oxidative stress (RONS formation) was shown for FOXO transcription factors [36, 37] and the circadian clock system (e.g. via SIRT-1) [50].

As summarized by Qin et al. [51], the circadian rhythm process relies on a group of clock genes such as the transcriptional activators circadian locomotor output cycles kaput (*Clock*), brain and muscle aryl hydrocarbon receptor nuclear translocator (*Arnt*)-like (*Bmal*) 1, period (*Per*) and cryptochrome (*Cry*) [52] and controls the time-dependent expression profile of multiple genes with the help of SIRT-1 and melatonin system [50]. The circadian rhythm is maintained by a transcription–translation feedback: the CLOCK/BMAL complex induces PER and CRY, suppressing the activity of the CLOCK/BMAL complex [53]. Recently, a molecular link of the circadian clock system with inflammation was shown via activation of the NFκB pathway [54] and *Cry1* and *Cry2* deletion aggravated arthritis by increased cytokine levels [55]. Also redox regulation of the circadian clock system was reported, mainly via SIRT-1, which is also reflected by a close interaction of oxidative stress with the circadian clock system in the aging process, heart disease, cancer, neurodegenerative diseases and diabetes [50]. In addition, a link between the circadian clock system and redox biology is implied by circadian rhythmicity of DNA repair proteins and antioxidant defense enzymes such as glutathione peroxide, superoxide dismutases, catalase and peroxiredoxins as well as levels of low molecular weight antioxidants such as ascorbate, uric acid and plasma thiols [50].

Effects of noise during sleep time on vascular function

Sleep deprivation has also been shown to cause a substantial inflammatory vessel phenotype as indicated by increased expression of IL-1β, IL-6, TNF-α, VCAM-1, ICAM-1 and E-selectin as well as augmented adhesion of monocytes to endothelial cells and NFκB activity [51]. These adverse inflammatory responses to sleep deprivation were associated with a loss of CRY-1 expression, a key protein of the circadian clock pathway, and the phenotype was rescued by in vivo adenoviral CRY-1 overexpression representing an example of successful “chronotherapy”. In addition, another study demonstrated a significant contribution

of sleep fragmentation to endothelial dysfunction, blood pressure increases, structural vascular changes, vascular senescence and recruitment of immune cells in mice [56]. Thus, these data may explain at least in part the significant increase in cardiovascular risk observed in patients with obstructive sleep apnea, being sleep fragmentation a hallmark of this disease [57]. In line with this increased risk, we observed endothelial dysfunction and eNOS uncoupling by S-glutathionylation in response to sleep noise exposure (**Figure 5**). Zweier and colleagues demonstrated that S-glutathionylation of eNOS is an important mechanism for eNOS uncoupling[58, 59], and we have shown that this occurs in diverse diseases including hypertension[60], diabetes[17], nitrate tolerance[61], aging[13], ischemia/reperfusion[62] and around-the-clock noise exposure[18].

In the present studies we also demonstrate that around-the-clock noise increases blood glucose levels potentially due to alterations in insulin signaling, which were previously reported to affect circadian clock genes [45]. The association between disrupted circadian rhythm and altered insulin signaling is further supported by human data on the adverse effects of sleep restriction on insulin sensitivity and the risk of diabetes [63-65]. Likewise, a large epidemiological study demonstrated that road traffic noise exposure, which is associated with sleep deprivation and fragmentation, is associated with an increased incidence of diabetes (population-based Danish Diet, Cancer and Health cohort of 57,053 people, 50-64 years of age) [66]. This was also shown by a prospective study on the effects of long-term aircraft noise exposure on body mass index, waist circumference, and risk of type 2 diabetes [67]. Our NGS data on alterations of protein phosphatases and calcium signaling provide may be also explained, at least in part, by changes in insulin sensitivity [41-44].

These observations are not surprising since the commonly used measurements of daytime noise have been suggested to be a source of exposure bias since during workdays most people spend their daytime hours out of the home and therefore nighttime noise measurements might alleviate any exposure bias problem.

Extended References

1. Schmidt F, Kolle K, Kreuder K, Schnorbus B, Wild P, Hechtner M, Binder H, Gori T, Munzel T. Nighttime aircraft noise impairs endothelial function and increases blood pressure in patients with or at high risk for coronary artery disease. Clin Res Cardiol 2015;**104**(1):23-30.
2. Turner JG, Parrish JL, Hughes LF, Toth LA, Caspary DM. Hearing in laboratory animals: strain differences and nonauditory effects of noise. Comp Med 2005;**55**(1):12-23.
3. Kane KA, Winslow E. Antidysrhythmic and electrophysiological effects of a new antianginal agent, bepridil. J Cardiovasc Pharmacol 1980;**2**(2):193-203.
4. Munzel T, Giaid A, Kurz S, Stewart DJ, Harrison DG. Evidence for a role of endothelin 1 and protein kinase C in nitroglycerin tolerance. Proc Natl Acad Sci 1995;**92**(11):5244-8.
5. Oelze M, Knorr M, Kroller-Schon S, Kossmann S, Gottschlich A, Rummler R, Schuff A, Daub S, Doppler C, Kleinert H, Gori T, Daiber A, Munzel T. Chronic therapy with isosorbide-5-mononitrate causes endothelial dysfunction, oxidative stress, and a marked increase in vascular endothelin-1 expression. Eur Heart J 2013;**34**(41):3206-16.
6. Oelze M, Kroller-Schon S, Welschof P, Jansen T, Hausding M, Mikhed Y, Stamm P, Mader M, Zinssius E, Agdauletova S, Gottschlich A, Steven S, Schulz E, Bottari SP, Mayoux E, Munzel T, Daiber A. The sodium-glucose co-transporter 2 inhibitor empagliflozin improves diabetes-induced vascular dysfunction in the streptozotocin diabetes rat model by interfering with oxidative stress and glucotoxicity. PLoS One 2014;**9**(11):e112394.
7. Zhu C, Herrmann US, Falsig J, Abakumova I, Nuvolone M, Schwarz P, Frauenknecht K, Rushing EJ, Aguzzi A. A neuroprotective role for microglia in prion diseases. J Exp Med 2016;**213**(6):1047-59.
8. Frauenknecht K, Katzav A, Grimm C, Chapman J, Sommer CJ. Neurological impairment in experimental antiphospholipid syndrome is associated with increased ligand binding to hippocampal and cortical serotonergic 5-HT1A receptors. Immunobiology 2013;**218**(4):517-26.
9. Oelze M, Daiber A, Brandes RP, Hortmann M, Wenzel P, Hink U, Schulz E, Mollnau H, von Sandersleben A, Kleschyov AL, Mulsch A, Li H, Forstermann U, Munzel T. Nebivolol inhibits superoxide formation by NADPH oxidase and endothelial dysfunction in angiotensin II-treated rats. Hypertension 2006;**48**(4):677-84.
10. Wenzel P, Schulz E, Oelze M, Muller J, Schuhmacher S, Alhamdani MS, Debrezion J, Hortmann M, Reifenberg K, Fleming I, Munzel T, Daiber A. AT1-receptor blockade by telmisartan upregulates GTP-cyclohydrolase I and protects eNOS in diabetic rats. Free Radic Biol Med 2008;**45**(5):619-26.
11. Oelze M, Knorr M, Schuhmacher S, Heeren T, Otto C, Schulz E, Reifenberg K, Wenzel P, Munzel T, Daiber A. Vascular dysfunction in streptozotocin-induced experimental diabetes strictly depends on insulin deficiency. J Vasc Res 2011;**48**(4):275-84.
12. Hirano K, Chen WS, Chueng AL, Dunne AA, Seredenina T, Filippova A, Ramachandran S, Bridges A, Chaudry L, Pettman G, Allan C, Duncan S, Lee KC, Lim J, Ma MT, Ong AB, Ye NY, Nasir S, Mulyanidewi S, Aw CC, Oon PP, Liao S, Li D, Johns DG, Miller ND, Davies CH, Browne ER, Matsuoka Y, Chen DW, Jaquet V, Rutter AR. Discovery of GSK2795039, a Novel Small Molecule NADPH Oxidase 2 Inhibitor. Antioxid Redox Signal 2015;**23**(5):358-74.
13. Oelze M, Kroller-Schon S, Steven S, Lubos E, Doppler C, Hausding M, Tobias S, Brochhausen C, Li H, Torzewski M, Wenzel P, Bachschmid M, Lackner KJ, Schulz E, Munzel T, Daiber A. Glutathione peroxidase-1 deficiency potentiates dysregulatory modifications of endothelial nitric oxide synthase and vascular dysfunction in aging. Hypertension 2014;**63**(2):390-6.

14. Bosmann M, Russkamp NF, Patel VR, Zetoune FS, Sarma JV, Ward PA. The outcome of polymicrobial sepsis is independent of T and B cells. Shock 2011;**36**(4):396-401.
15. Daiber A, August M, Baldus S, Wendt M, Oelze M, Sydow K, Kleschyov AL, Munzel T. Measurement of NAD(P)H oxidase-derived superoxide with the luminol analogue L-012. Free Radic Biol Med 2004;**36**(1):101-11.
16. Zhao H, Joseph J, Fales HM, Sokoloski EA, Levine RL, Vasquez-Vivar J, Kalyanaraman B. Detection and characterization of the product of hydroethidine and intracellular superoxide by HPLC and limitations of fluorescence. Proc Natl Acad Sci U S A 2005;**102**(16):5727-32.
17. Schuhmacher S, Oelze M, Bollmann F, Kleinert H, Otto C, Heeren T, Steven S, Hausding M, Knorr M, Pautz A, Reifenberg K, Schulz E, Gori T, Wenzel P, Munzel T, Daiber A. Vascular dysfunction in experimental diabetes is improved by pentaerithrityl tetranitrate but not isosorbide-5-mononitrate therapy. Diabetes 2011;**60**(10):2608-16.
18. Munzel T, Daiber A, Steven S, Tran LP, Ullmann E, Kossmann S, Schmidt FP, Oelze M, Xia N, Li H, Pinto A, Wild P, Pies K, Schmidt ER, Rapp S, Kroller-Schon S. Effects of noise on vascular function, oxidative stress, and inflammation: mechanistic insight from studies in mice. Eur Heart J 2017;**38**(37):2838-2849.
19. Hausding M, Jurk K, Daub S, Kroller-Schon S, Stein J, Schwenk M, Oelze M, Mikhed Y, Kerahrodi JG, Kossmann S, Jansen T, Schulz E, Wenzel P, Reske-Kunz AB, Becker C, Munzel T, Grabbe S, Daiber A. CD40L contributes to angiotensin II-induced pro-thrombotic state, vascular inflammation, oxidative stress and endothelial dysfunction. Basic Res Cardiol 2013;**108**(6):386.
20. Feng M, Whitesall S, Zhang Y, Beibel M, D'Alecy L, DiPetrillo K. Validation of volume-pressure recording tail-cuff blood pressure measurements. Am J Hypertens 2008;**21**(12):1288-91.
21. Dobin A, Davis CA, Schlesinger F, Drenkow J, Zaleski C, Jha S, Batut P, Chaisson M, Gingeras TR. STAR: ultrafast universal RNA-seq aligner. Bioinformatics 2013;**29**(1):15-21.
22. Li B, Dewey CN. RSEM: accurate transcript quantification from RNA-Seq data with or without a reference genome. BMC bioinformatics 2011;**12**:323.
23. Team RC. R: A Language and Environment for Statistical Computing. Vienna, Austria 2016.
24. Love MI, Huber W, Anders S. Moderated estimation of fold change and dispersion for RNA-seq data with DESeq2. Genome biology 2014;**15**(12):550.
25. Ogata H, Goto S, Sato K, Fujibuchi W, Bono H, Kanehisa M. KEGG: Kyoto Encyclopedia of Genes and Genomes. Nucleic acids research 1999;**27**(1):29-34.
26. Kanehisa M, Sato Y, Kawashima M, Furumichi M, Tanabe M. KEGG as a reference resource for gene and protein annotation. Nucleic acids research 2016;**44**(D1):D457-62.
27. Luo W, Brouwer C. Pathview: an R/Bioconductor package for pathway-based data integration and visualization. Bioinformatics 2013;**29**(14):1830-1.
28. Greene CS, Krishnan A, Wong AK, Ricciotti E, Zelaya RA, Himmelstein DS, Zhang R, Hartmann BM, Zaslavsky E, Sealfon SC, Chasman DI, FitzGerald GA, Dolinski K, Grosser T, Troyanskaya OG. Understanding multicellular function and disease with human tissue-specific networks. Nature genetics 2015;**47**(6):569-76.
29. Faul F, Erdfelder E, Lang AG, Buchner A. G*Power 3: a flexible statistical power analysis program for the social, behavioral, and biomedical sciences. Behav Res Methods 2007;**39**(2):175-91.
30. Babisch W. Cardiovascular effects of noise. Noise & health 2011;**13**(52):201-4.
31. Chan SH, Chan JY. Angiotensin-generated reactive oxygen species in brain and pathogenesis of cardiovascular diseases. Antioxid Redox Signal 2013;**19**(10):1074-84.

32. Said MA, El-Gohary OA. Effect of noise stress on cardiovascular system in adult male albino rat: implication of stress hormones, endothelial dysfunction and oxidative stress. General physiology and biophysics 2016;**35**(3):371-7.
33. Selander J, Bluhm G, Theorell T, Pershagen G, Babisch W, Seiffert I, Houthuijs D, Breugelmans O, Vigna-Taglianti F, Antoniotti MC, Velonakis E, Davou E, Dudley ML, Jarup L, Consortium H. Saliva cortisol and exposure to aircraft noise in six European countries. Environmental health perspectives 2009;**117**(11):1713-7.
34. Christensen JS, Hjortebjerg D, Raaschou-Nielsen O, Ketzel M, Sorensen TI, Sorensen M. Pregnancy and childhood exposure to residential traffic noise and overweight at 7 years of age. Environ Int 2016;**94**:170-6.
35. Christensen JS, Raaschou-Nielsen O, Tjonneland A, Overvad K, Nordsborg RB, Ketzel M, Sorensen T, Sorensen M. Road Traffic and Railway Noise Exposures and Adiposity in Adults: A Cross-Sectional Analysis of the Danish Diet, Cancer, and Health Cohort. Environmental health perspectives 2016;**124**(3):329-35.
36. Klotz LO, Sanchez-Ramos C, Prieto-Arroyo I, Urbanek P, Steinbrenner H, Monsalve M. Redox regulation of FoxO transcription factors. Redox biology 2015;**6**:51-72.
37. Urbanek P, Klotz LO. Posttranscriptional regulation of FOXO expression: microRNAs and beyond. Br J Pharmacol 2016.
38. Schenk H, Klein M, Erdbrugger W, Droge W, Schulze-Osthoff K. Distinct effects of thioredoxin and antioxidants on the activation of transcription factors NF-kappa B and AP-1. Proc Natl Acad Sci U S A 1994;**91**(5):1672-6.
39. Schreck R, Albermann K, Baeuerle PA. Nuclear factor kappa B: an oxidative stress-responsive transcription factor of eukaryotic cells (a review). Free radical research communications 1992;**17**(4):221-37.
40. Mikhed Y, Gorlach A, Knaus UG, Daiber A. Redox regulation of genome stability by effects on gene expression, epigenetic pathways and DNA damage/repair. Redox biology 2015;**5**:275-89.
41. Tremblay ML, Giguere V. Phosphatases at the heart of FoxO metabolic control. Cell metabolism 2008;**7**(2):101-3.
42. Wu X, Zhu L, Zilbering A, Mahadev K, Motoshima H, Yao J, Goldstein BJ. Hyperglycemia potentiates H(2)O(2) production in adipocytes and enhances insulin signal transduction: potential role for oxidative inhibition of thiol-sensitive protein-tyrosine phosphatases. Antioxid Redox Signal 2005;**7**(5-6):526-37.
43. Hsu MF, Meng TC. Enhancement of insulin responsiveness by nitric oxide-mediated inactivation of protein-tyrosine phosphatases. J Biol Chem 2010;**285**(11):7919-28.
44. Rotter D, Grinsfelder DB, Parra V, Pedrozo Z, Singh S, Sachan N, Rothermel BA. Calcineurin and its regulator, RCAN1, confer time-of-day changes in susceptibility of the heart to ischemia/reperfusion. J Mol Cell Cardiol 2014;**74**:103-11.
45. Chaves I, van der Horst GT, Schellevis R, Nijman RM, Koerkamp MG, Holstege FC, Smidt MP, Hoekman MF. Insulin-FOXO3 signaling modulates circadian rhythms via regulation of clock transcription. Curr Biol 2014;**24**(11):1248-55.
46. Kanazawa LK, Vecchia DD, Wendler EM, Hocayen PA, Dos Reis Livero FA, Stipp MC, Barcaro IM, Acco A, Andreatini R. Quercetin reduces manic-like behavior and brain oxidative stress induced by paradoxical sleep deprivation in mice. Free Radic Biol Med 2016;**99**:79-86.
47. Alzoubi KH, Khabour OF, Albawaana AS, Alhashimi FH, Athamneh RY. Tempol prevents chronic sleep-deprivation induced memory impairment. Brain research bulletin 2016;**120**:144-50.
48. Schiavone S, Jaquet V, Trabace L, Krause KH. Severe life stress and oxidative stress in the brain: from animal models to human pathology. Antioxid Redox Signal 2013;**18**(12):1475-90.

49. Kan H, Hu W, Wang Y, Wu W, Yin Y, Liang Y, Wang C, Huang D, Li W. NADPH oxidase-derived production of reactive oxygen species is involved in learning and memory impairments in 16-month-old female rats. Molecular medicine reports 2015;**12**(3):4546-53.
50. Wilking M, Ndiaye M, Mukhtar H, Ahmad N. Circadian rhythm connections to oxidative stress: implications for human health. Antioxid Redox Signal 2013;**19**(2):192-208.
51. Qin B, Deng Y. Overexpression of circadian clock protein cryptochrome (CRY) 1 alleviates sleep deprivation-induced vascular inflammation in a mouse model. Immunol Lett 2015;**163**(1):76-83.
52. Cuninkova L, Brown SA. Peripheral circadian oscillators: interesting mechanisms and powerful tools. Ann N Y Acad Sci 2008;**1129**:358-70.
53. Sato TK, Yamada RG, Ukai H, Baggs JE, Miraglia LJ, Kobayashi TJ, Welsh DK, Kay SA, Ueda HR, Hogenesch JB. Feedback repression is required for mammalian circadian clock function. Nature genetics 2006;**38**(3):312-9.
54. Narasimamurthy R, Hatori M, Nayak SK, Liu F, Panda S, Verma IM. Circadian clock protein cryptochrome regulates the expression of proinflammatory cytokines. Proc Natl Acad Sci U S A 2012;**109**(31):12662-7.
55. Hashiramoto A, Yamane T, Tsumiyama K, Yoshida K, Komai K, Yamada H, Yamazaki F, Doi M, Okamura H, Shiozawa S. Mammalian clock gene Cryptochrome regulates arthritis via proinflammatory cytokine TNF-alpha. J Immunol 2010;**184**(3):1560-5.
56. Carreras A, Zhang SX, Peris E, Qiao Z, Gileles-Hillel A, Li RC, Wang Y, Gozal D. Chronic sleep fragmentation induces endothelial dysfunction and structural vascular changes in mice. Sleep 2014;**37**(11):1817-24.
57. Wang J, Yu W, Gao M, Zhang F, Gu C, Yu Y, Wei Y. Impact of Obstructive Sleep Apnea Syndrome on Endothelial Function, Arterial Stiffening, and Serum Inflammatory Markers: An Updated Meta-analysis and Metaregression of 18 Studies. Journal of the American Heart Association 2015;**4**(11).
58. Chen CA, Wang TY, Varadharaj S, Reyes LA, Hemann C, Talukder MA, Chen YR, Druhan LJ, Zweier JL. S-glutathionylation uncouples eNOS and regulates its cellular and vascular function. Nature 2010;**468**(7327):1115-8.
59. Zweier JL, Chen CA, Druhan LJ. S-glutathionylation reshapes our understanding of endothelial nitric oxide synthase uncoupling and nitric oxide/reactive oxygen species-mediated signaling. Antioxid Redox Signal 2011;**14**(10):1769-75.
60. Kroller-Schon S, Steven S, Kossmann S, Scholz A, Daub S, Oelze M, Xia N, Hausding M, Mikhed Y, Zinssius E, Mader M, Stamm P, Treiber N, Scharffetter-Kochanek K, Li H, Schulz E, Wenzel P, Munzel T, Daiber A. Molecular mechanisms of the crosstalk between mitochondria and NADPH oxidase through reactive oxygen species-studies in white blood cells and in animal models. Antioxid Redox Signal 2014;**20**(2):247-66.
61. Knorr M, Hausding M, Kroller-Schuhmacher S, Steven S, Oelze M, Heeren T, Scholz A, Gori T, Wenzel P, Schulz E, Daiber A, Munzel T. Nitroglycerin-induced endothelial dysfunction and tolerance involve adverse phosphorylation and S-Glutathionylation of endothelial nitric oxide synthase: beneficial effects of therapy with the AT1 receptor blocker telmisartan. Arterioscler Thromb Vasc Biol 2011;**31**(10):2223-31.
62. De Pascali F, Hemann C, Samons K, Chen CA, Zweier JL. Hypoxia and reoxygenation induce endothelial nitric oxide synthase uncoupling in endothelial cells through tetrahydrobiopterin depletion and S-glutathionylation. Biochemistry 2014;**53**(22):3679-88.
63. Buxton OM, Pavlova M, Reid EW, Wang W, Simonson DC, Adler GK. Sleep restriction for 1 week reduces insulin sensitivity in healthy men. Diabetes 2010;**59**(9):2126-2133.

64. Cappuccio FP, D'Elia L, Strazzullo P, Miller MA. Quantity and quality of sleep and incidence of type 2 diabetes: a systematic review and meta-analysis. Diabetes care 2010;**33**(2):414-420.
65. Spiegel K, Tasali E, Leproult R, Van Cauter E. Effects of poor and short sleep on glucose metabolism and obesity risk. Nature reviews Endocrinology 2009;**5**(5):253-61.
66. Sorensen M, Andersen ZJ, Nordsborg RB, Becker T, Tjonneland A, Overvad K, Raaschou-Nielsen O. Long-term exposure to road traffic noise and incident diabetes: a cohort study. Environmental health perspectives 2013;**121**(2):217-22.
67. Eriksson C, Hilding A, Pyko A, Bluhm G, Pershagen G, Ostenson CG. Long-term aircraft noise exposure and body mass index, waist circumference, and type 2 diabetes: a prospective study. Environmental health perspectives 2014;**122**(7):687-94.